

AD 480 846

480846

Low Density Ablation Materials Survey

JANUARY 1966

Prepared by W.E. WELSH and K.E. STARNER
Aerodynamics and Propulsion Research Laboratory
and
D.H. LEEDS and J.I. SLAUGHTER
Materials Sciences Laboratory

Prepared for **BALLISTIC SYSTEMS AND SPACE SYSTEMS DIVISIONS**
AIR FORCE SYSTEMS COMMAND
LOS ANGELES AIR FORCE STATION
Los Angeles, California



LABORATORY OPERATIONS • AEROSPACE CORPORATION
CONTRACT NO. AF 04(695)-669

NOTICE

This document is subject to special export controls and each transmittal to foreign governments or foreign nationals may be made only with prior approval of SSD (SSTRT).

SSD-TR-66-35

Report No.
FDR-669(6240-10)-5

LOW DENSITY ABLATION MATERIALS SURVEY *

Prepared by

W. E. Welsh and K. E. Starner
Aerodynamics and Propulsion Research Laboratory
and
D. H. Leeds and J. I. Slaughter
Materials Sciences Laboratory

Laboratory Operations
AEROSPACE CORPORATION
El Segundo, California

Contract No. AF 04(695)-669

January 1966

Prepared for

BALLISTIC SYSTEMS AND SPACE SYSTEMS DIVISIONS
AIR FORCE SYSTEMS COMMAND
LOS ANGELES AIR FORCE STATION
Los Angeles, California

LOW DENSITY ABLATION MATERIALS SURVEY

Prepared

W. E. Welsh
W. E. Welsh

D. H. Leeds
D. H. Leeds

K. E. Starnes
K. E. Starnes

J. I. Slaughter
J. I. Slaughter, Head
Re-entry Effects Department

Approved

H. Mirels
H. Mirels, Head
Aerodynamics and Heat
Transfer Department

W. C. Riley
W. C. Riley, Assoc. Director
Materials Sciences Laboratory

J. G. Logan
J. G. Logan, Director
Aerodynamics and Propulsion
Research Laboratory

This technical documentary report has been reviewed and is approved for publication and dissemination. The conclusions and findings contained herein do not necessarily represent an official Air Force position.

For Space Systems Division
Air Force Systems Command

Robert F. Jones
Robert F. Jones, Captain
USAF

ABSTRACT

A survey of 12 low density ablators for thermal protection of lifting reentry vehicle surfaces was conducted jointly by AFML-Wright Field and the Aerospace Corporation. Eighty-nine arc tunnel tests were performed in the facility at Giannini Scientific Corporation, Santa Ana, California. The primary series of tests was performed to determine temperature response- and recession-characteristics at cold wall calorimeter heat flux levels of 20, 60, 90, 120, and 150 Btu/ft² sec. A second series of tests was performed to indicate the response of lowdensity ablators to aerodynamic shear. The results of these tests are evaluated relative to the thermal protection requirements for ablative lifting bodies for reentry systems.

The materials tested were found to have insulating characteristics comparable to idealized heat conductors with thermal diffusivities between 2 and 7×10^{-6} ft²/sec in the nonrecession regime. In some materials the apparent diffusivity tended to rise during the test. In the range of heat fluxes where surface recession occurred, only small differences in recessions were observed between materials. Two materials receded at a heat flux of 60 Btu/ft² sec, whereas the other materials did not recede at heat flux levels below 90 Btu/ft² sec.

This report is divided into four parts: Part 1. Introduction; Part 2. Test Procedure; Part 3. Aerothermodynamic Results and Analysis, and Part 4. Summary and Conclusions.

ACKNOWLEDGEMENT

The authors would like to express their appreciation to the following persons and firms who supplied the test materials:

Mr. C. M. Dolan, General Electric Company
Mr. D. L. Kummer, McDonnell Aircraft Corporation
Mr. D. V. Sallis, Martin Company
Mr. W. A. Brooks, NASA/Langley Research Center
Mr. R. B. Erb, NASA/Manned Space Flight Center
Dr. R. Feldman, Emerson Electric of St. Louis
Mr. R. M. Beasley, Lockheed Missiles and Space Company
Mr. E. Offenhartz, Avco-RAD

In addition, we especially wish to thank Lt. M. Jolly and Mr. L. Hjelm of WPAFB/AFML and Mr. Jim Todd and other personnel of the Giannini Scientific Corporation for conducting the tests.

CONTENTS

PART 1. INTRODUCTION	1-1
PART 2. TEST PROCEDURE	2-1
I. INTRODUCTION.....	2-1
II. EXPERIMENTAL PROCEDURE	2-4
A. Preliminary Testing	2-4
B. Materials Descriptions	2-5
C. Sample Preparation	2-8
D. Test Procedures	2-8
E. Calibration	2-11
REFERENCES	2-18
PART 3. AEROTHERMODYNAMIC RESULTS AND ANALYSIS	3-1
I. INTRODUCTION	3-1
II. RECESSION RATE	3-2
III. TEMPERATURE MEASUREMENTS	3-3
A. Front Surface Temperature	3-3
B. Rear-Face Temperature	3-6
C. Internal Temperatures	3-11
IV. CHAR DEPTH MEASUREMENTS	3-15
V. THERMAL RESPONSE ANALYSIS	3-15
VI. RECESSION ANALYSIS	3-29
VII. SHEAR TESTS	3-31
VIII. SUMMARY	3-32
REFERENCES	3-34

CONTENTS (Continued)

PART 4. SUMMARY AND CONCLUSIONS	4-1
I. SUMMARY	4-1
II. CONCLUSIONS AND RECOMMENDATIONS	4-10
REFERENCES	4-12

FIGURES

1-1	Typical Heat Balance for Low Density Elastomeric Ablator Plasma Arc Test at Moderate Heat Flux Showing Low Net Input to Substructure	1-2
1-2	Weight Comparison of Low Density Ablators with Standard Ablators for Typical Lifting Body Orbital Reentry Conditions, 400° F Backface Temperature	1-4
1-3	SV-5D Configuration, Artist's Conception	1-5
2-1	Materials Test Sample Configuration	2-2
2-2	Giannini Scientific Corporation 1 MW, Mach 3 Test Chamber	2-3
2-3	Aerospace Calorimeter Construction	2-14
2-4	Martin Transient Calorimeters	2-16
3-1	Front Surface Recession Rate	3-4
3-2	Front Surface Brightness Temperature	3-5
3-3	Rear-Face Temperature Response at $q_0 = 20 \text{ Btu/ft}^2\text{sec}$	3-7
3-4	Rear-Face Temperature Response at $q_0 = 60 \text{ Btu/ft}^2\text{sec}$	3-8
3-5	Rear-Face Temperature Response at $q_0 = 90 \text{ Btu/ft}^2\text{sec}$	3-9
3-6	Rear-Face Temperature Response at $q_0 = 120$ and $150 \text{ Btu/ft}^2\text{sec}$	3-10
3-7	Temperature Response at 1 in. Depth, $q_0 = 20$ and $60 \text{ Btu/ft}^2\text{sec}$	3-12
3-8	Temperature Response at 1 in. Depth, $q_0 = 90$ and $120 \text{ Btu/ft}^2\text{sec}$	3-13
3-9	Temperature Response at 1 in. Depth, $q_0 = 150 \text{ Btu/ft}^2\text{sec}$	3-14
3-10	Infinite Plate Conduction Solution	3-18
3-11	Comparison of Thermal Response	3-20
3-12	Theoretical Error in E Based on Half-Depth Temperature	3-22
3-13	Theoretical Insulation Efficiency	3-24

FIGURES (Continued)

3-14	Experimental Insulation Efficiency	3-26
3-15	Rear-Face Temperature Rise, $q_0 = 20 \text{ Btu/ft}^2\text{sec}$	3-28
3-16	Recession Characteristics	3-30
4-1	Recession Characteristics of Low Density Ablators (52 lb/ft^3)	4-4
4-2	Insulation Efficiency of NASA/Langley Purple Blend with Fiber Addition	4-8

TABLES

2-1	Materials Tested	2-1
2-2	Calibration Results	2-10
3-1	Char Thickness Measurements	3-16
4-1	Mass Loss Data on Charred Silicone Elastomer at 0.033 atm	4-6
4-2	Rate Data on Charred Silicone Elastomer at 0.033 atm . .	4-7

PART 1. INTRODUCTION

Recent advances in ablation analysis, materials formulation, and manufacturing methods leading to a new class of low density ablative materials have been coupled with the development of compatible manned and unmanned lifting reentry configurations that permit maneuvering reentry and controlled landing at a selected land base. These vehicles are potentially reusable with minimum refurbishment, are economical and reliable, and have growth potential with regard to payload capability and size.

Extensive Air Force and NASA aerodynamic wind tunnel configuration studies have demonstrated that it is possible to design lifting body vehicles with supersonic L to D of approximately 1.3 and a cross-range maneuver capability greater than 700 n mi. These shapes are simpler and have better volumetric efficiency than the configurations with supersonic L to D ~ 3 . Additionally, vehicles with L to D ≈ 1.3 have a subsonic L to D of slightly above 3, well within the range of pilot capability for horizontal landing.

Also, other Air Force and NASA sponsored programs have demonstrated that the low density ablation materials are simpler to process, more reliable, permit greater mission flexibility, and will take a high heat flux overshoot without catastrophic failure as compared to state of the art coated refractory metals.

The importance of low density ablation materials to lifting reentry is illustrated by the heat balance shown in Fig. 1-1 for a typical plasma test. The calculations show the low net heat input into the material and substructure under typical flight conditions and indicate that the low density materials are primarily a convenient-to-manufacture combination of a re-radiative-insulative system for the moderate heat fluxes encountered in lifting reentry. The lower heat fluxes encountered on upper and aft surfaces of these vehicles could be accommodated by re-radiative systems, e.g., TZM coated molybdenum can be used to 42.5 Btu/ft²/sec, D-6 coated columbium to 35.8 Btu/ft²/sec, and Rene-41 to 11 Btu/ft²/sec. The best

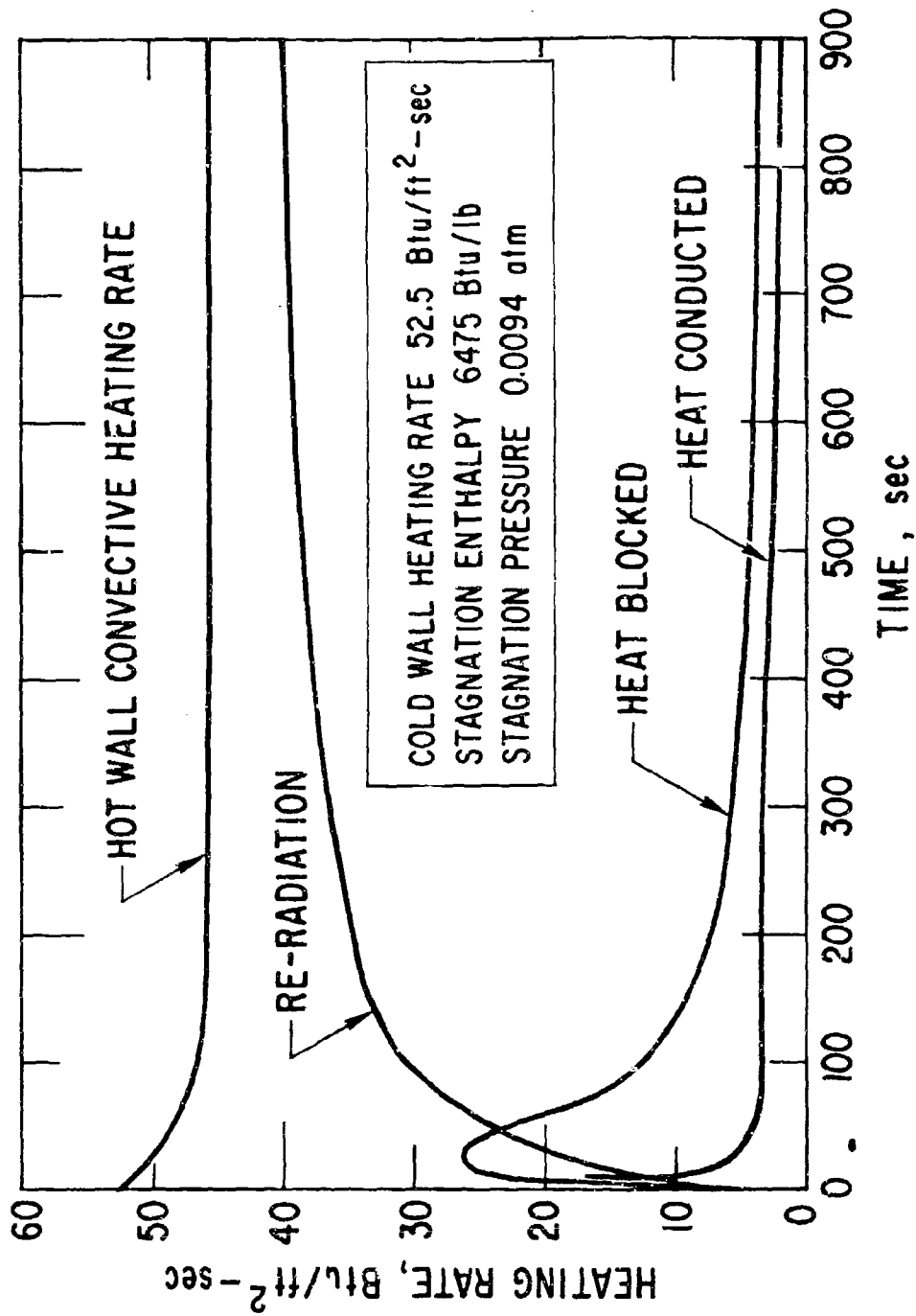


Fig. 1-1. Typical Heat Balance for Low Density Elastomeric Ablator Plasma Arc Test at Moderate Heat Flux Showing Low Net Input to Substructure

combination of materials for structural and heat protection systems is the subject of continuing Air Force and NASA study programs; however, it is clear that the low density materials are important to the development of the technology of manned lifting reentry and for general aerospace ablative insulation use.

The efficiency of the low density materials in relation to conventional high density ablative materials is shown in Fig. 1-2 where integrated total heat is plotted vs thermal protection weight required for phenolic-refrasil, phenolic-nylon, and low density ablators. In view of the high total heat input for the long reentry time associated with lifting reentry, the low density ablators are lighter weight and make possible a reasonable ratio of heat shield to total system weight.

The Space Systems Division of the Air Force is engaged in a program to flight test a maneuverable lifting body vehicle as part of the START Program. This project, called PRIME, is a four flight hypersonic test program in which low earth orbit reentry conditions are simulated. Figure 1-3 shows the complex contour of the vehicle.

The tests described in this report were conducted for the Air Force Space Systems Division to evaluate the thermal performance and in a general way the potential systems applications of a large variety of low density ablators for present and future reentry missions. These materials were developed under NASA, Air Force, and company-sponsored programs and were made available to Aerospace for these tests by either the sponsoring agency or the materials supplier. The purpose of the tests was to aid in the development of improved thermal protection systems for ablative lifting bodies for manned reentry.

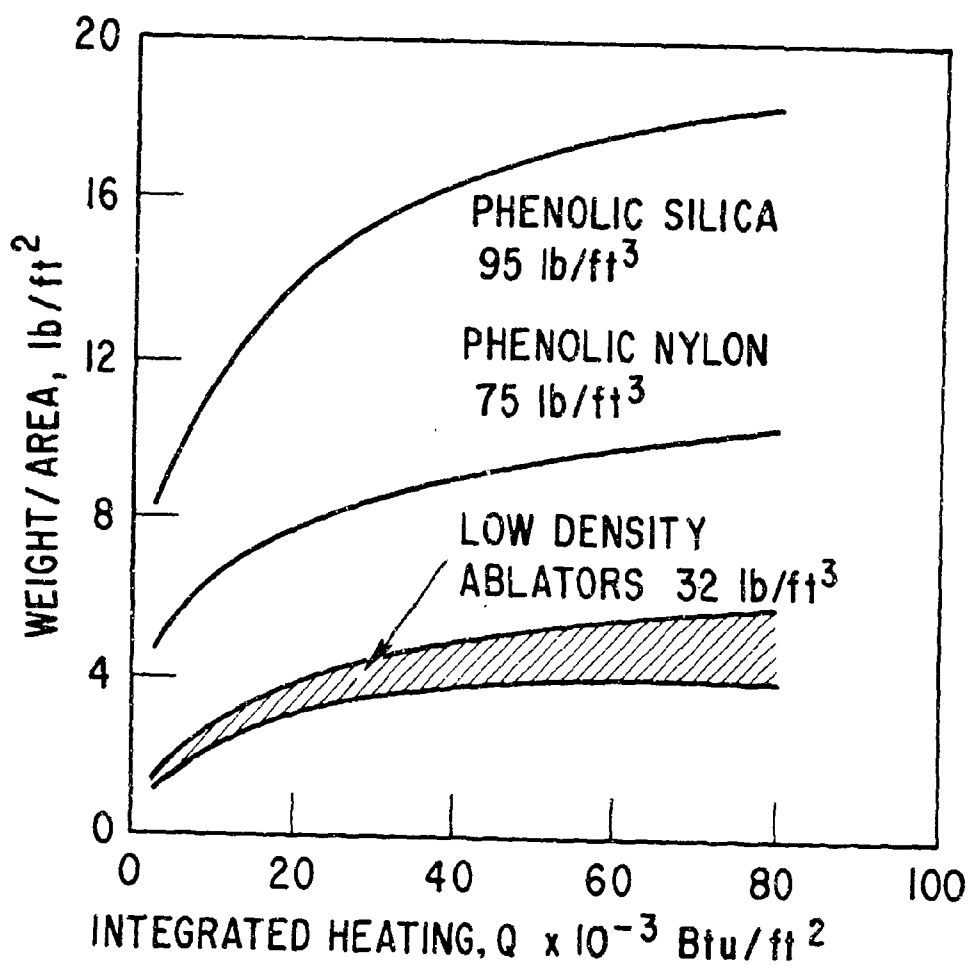


Fig. 1-2. Weight Comparison of Low Density Ablators with Standard Ablators for Typical Lifting Body Orbital Reentry Conditions, 400°F Backface Temperature



Fig. 1-3. SV-5D Configuration, Artist's Conception

PART 2. TEST PROCEDURE

I. INTRODUCTION

A series of low density ablator plasma arc tests was conducted at Giannini Scientific Corporation in collaboration with the Air Force Materials Laboratory. These tests were performed at cold wall heat fluxes of 20, 60, 90, 120, and 150 Btu/ft² sec on the ablator systems listed in Table 2-1. The data for the Martin material, ESA 3560H and ESA 3560HF, are reported in a separate classified document (Ref. 3-1).

Table 2-1. Materials Tested

Material No.	Supplier	Suppliers Specification	Material Type
1	G. E.	ESM 1001 (honeycomb)	elastomer
2A	Lockheed	Lockheat 1	inorganic laminate
2C	Lockheed	Lockheat 2	inorganic laminate
3	G. E.	ESM 1004 (no honeycomb)	elastomer
4	McDonnell	S-6 3/16 cell	elastomer
5	McDonnell	S-6 3/8 cell	elastomer
6	Avco	5026-39	rigid composite
7	Martin	ESA 3560H	elastomer
8	Emerson	T-500-111	rigid composite
9	Langley	Purple Blend	elastomer
10	Langley	Phenolic Nylon	rigid composite
11	Martin	ESA 3560HF	elastomer

The equipment used for these tests was a 900 kW reconstituted air plasma arc (79% N₂, 21% O₂), an uncooled sample holder mounted in a water cooled sting, a manual pyrometer, a movie camera, and a multichannel millivolt recorder to measure temperatures 1 in. behind the hot face and at the rear face. Figure 2-1 shows the sample configuration and Fig. 2-2 the test facility arrangement.

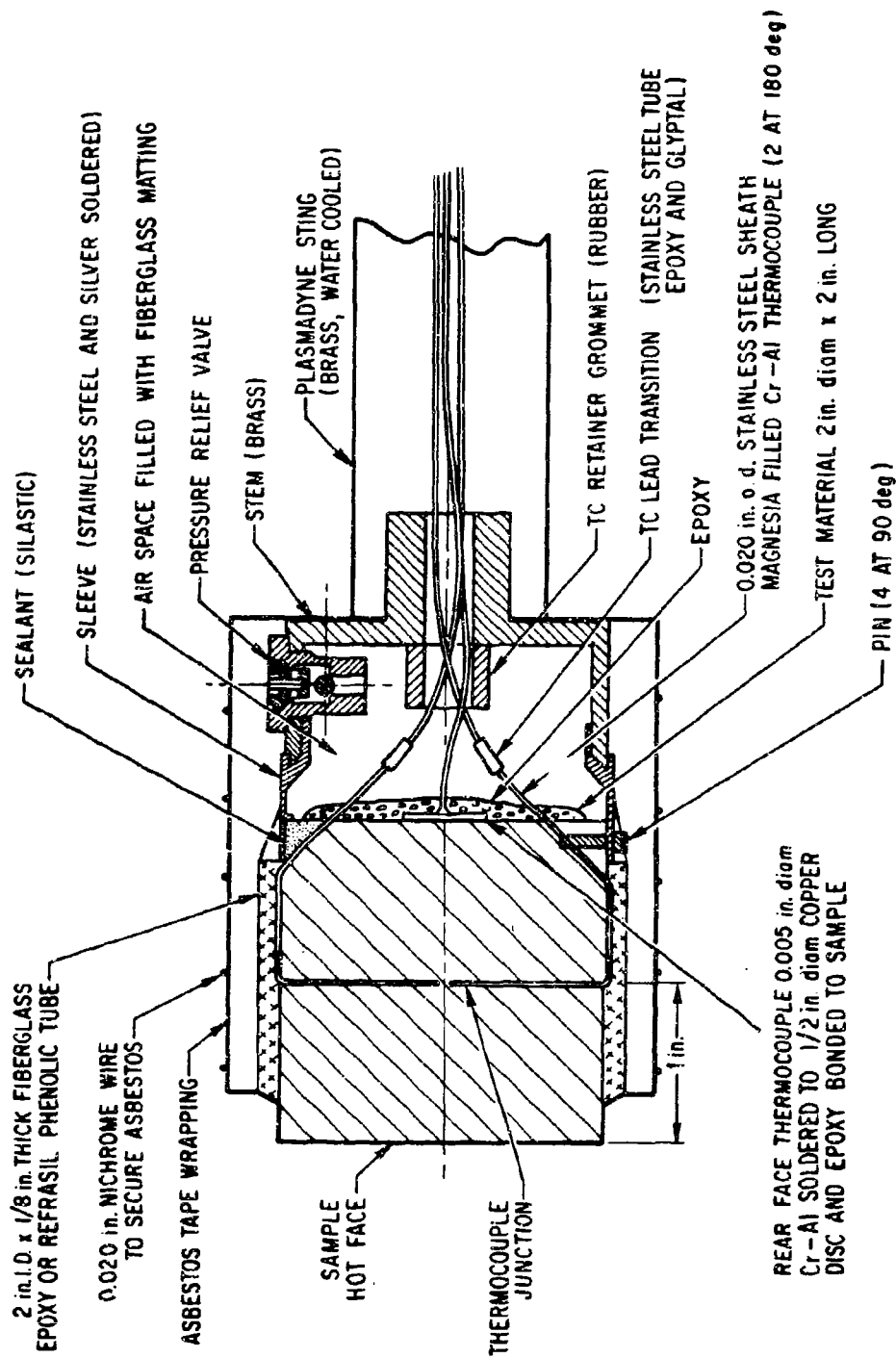


Fig. 2-1. Materials Test Sample Configuration

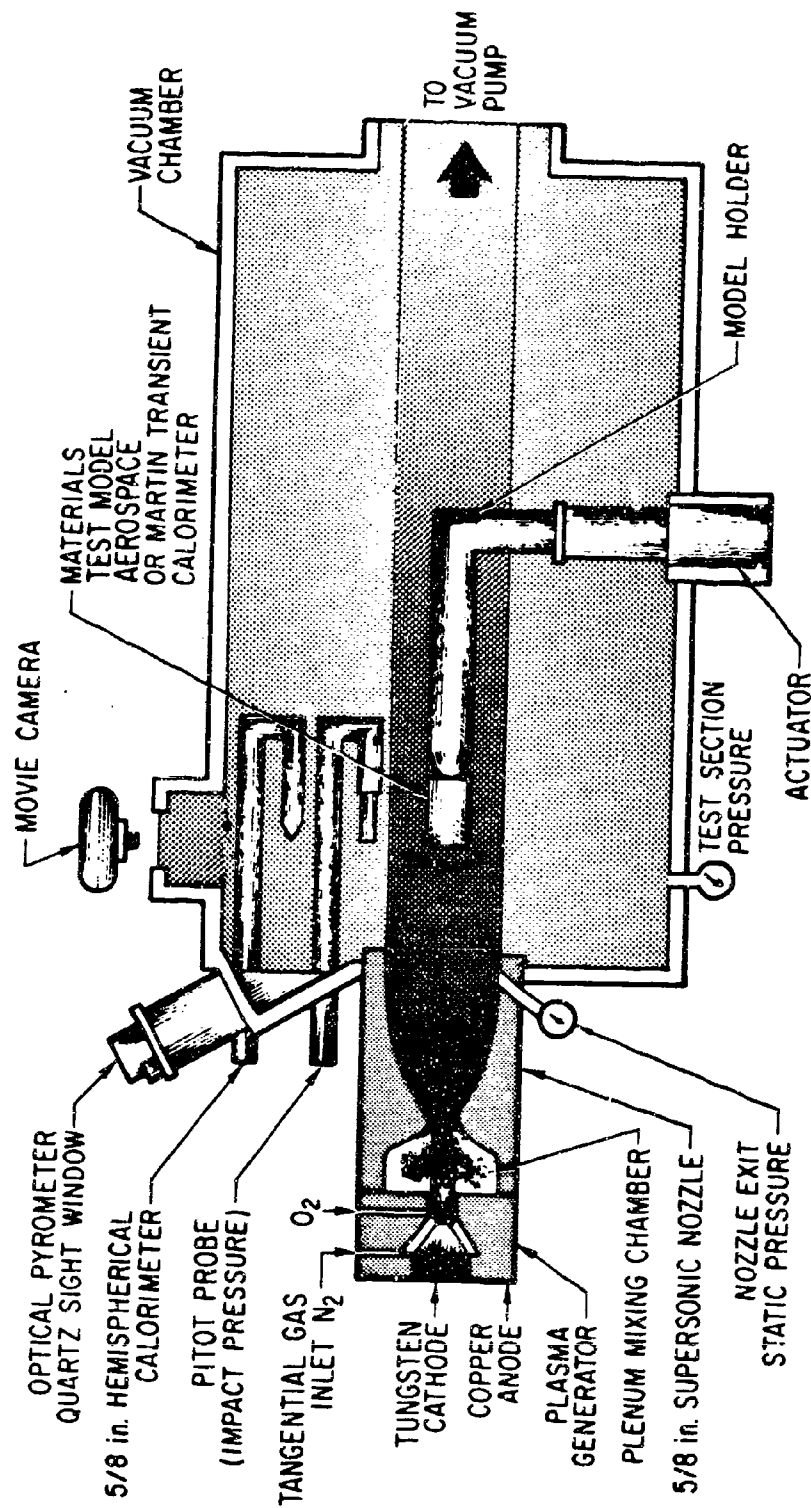


Fig. 2-2. Giannini Scientific Corporation 1 MW, Mach 3 Test Chamber

The plasma arc used a tungsten-tipped copper cathode and a copper anode operating in the range 130 to 300 V and 440 to 1200 A as determined by the heat flux level desired. The plenum chamber between the anode and the exhaust nozzle promotes mixing and uniform outlet flow.

The Mach 3 nozzle used in these tests had a 5.125 in. exit diameter, an 8 to 1 area ratio, a rounded inlet contour, and a sharp edged outlet and was 8 in. long. The nozzle was enclosed in a 30-in. diam test chamber which had two 6-in. diam ports for visual observation of the tests and for photography. Additionally, a window 45 deg to the axis of the plasma flow was used for optical pyrometer temperature readings. The vacuum system was ducted through a vacuum blowdown tank. The total capacity of the pumps used during the tests was 5000 cfm, although 9000 cfm was available.

Nominal enthalpy values of 10,000 Btu/lb were used to simulate the flight environment. The corresponding model stagnation pressures for the Mach 3, 5-1/8 in. nozzle varied between 2 and 20 mm Hg. Although these model pressures do not simulate flight conditions exactly, it was felt that pressure was the least sensitive test parameter.

II. EXPERIMENTAL PROCEDURE

A. PRELIMINARY TESTING

Preliminary testing was carried out at Giannini Scientific Corporation with both elastomeric and rigid composite materials samples instrumented with chromel-alumel thermocouples located 1/4, 1/2, 1, and 2 in. from the hot face. These tests, performed at a heat flux of 60 Btu/ft² sec, an enthalpy of 5000 Btu/lb, and a pressure of approximately 10⁻⁴ atm, showed good correlation with calculated temperature-time histories obtained from the Aerospace Corporation charring-ablator computer program. The results of these tests indicated that the model holder design was satisfactory and that the best test condition was achieved in the 5 in. diam plasma flow as compared

to the smaller Giannini plasma arcs. To simplify fabrication and instrumentation, it was decided that only three thermocouples would be used. Two were placed along the isotherm 1 in. from the hot face with adjacent junctions 1/8 in. off the center of the specimen, and one was placed at the rear face (Fig. 2-1).

After the model geometry and the plasma test facility were selected, the operating conditions of the arc were modified to achieve the desired nominal enthalpy of 10,000 Btu/lb. This change may have inadvertently caused some of the experimental difficulties with side and backface heating, as discussed later.

B. MATERIALS DESCRIPTIONS

The materials listed in Table 2-1 are described below. The proprietary materials descriptions are indicated by quotes taken from correspondence with the supplier. Specimen density of all materials tested was in the range from 30 to 35 lb/ft³, to minimize the influence of density differences on insulation performance.

1. MATERIAL 1

General Electric's ESM 1001, according to Dolan (Ref. 2-1), is an RTV-60 silicone elastomeric resin system with 4.3% asbestos and 0.8% glass filler materials foamed into a slit phenolic-fiberglass honeycomb. The slit honeycomb gives adequate flexibility for application of the material over complex surfaces but retains the reinforcing and structural bonding advantages of regular honeycomb reinforced materials.

2. MATERIALS 2A AND 2C

"The Lockheed Missiles and Space Company samples were built from ceramic inorganic insulation, having a density of 9-10 lb/ft³. Exterior surfaces were covered with high density silica fibers and ceramic binders. Outer surface thicknesses were selected to bring the average density of the specimen to the specified density of 32 lb/ft³. The samples represent an all-inorganic composite material specifically designed for thermal protection applications below 60 Btu/ft² sec."

3. MATERIAL 3

The ESM 1004 without honeycomb, according to Dolan (Ref. 2-1), is an RTV-560 foamed phenyl silicone base elastomeric resin system with 12% aluminum silicate fibers as filler material.

4. MATERIALS 4 AND 5

"The McDonnell Aircraft Corporation's S-6 ablative material is a foamed, filled silicone elastomer. Density can be varied between 17 and 50 lb/ft³. A low stiffening point elastomer may be utilized if very low temperatures are to be encountered. Material 4 was contained in a 3/16 in. cell phenolic-fiberglass core that had a density of 5.5 lb/ft³. Material 5 used a 3/8 in. cell phenolic-fiberglass core that had a density of 6.0 lb/ft³."

5. MATERIAL 6

"Avcoat 5026-39 designates a fabricated form of one of Avco's low density charring ablator systems. This material comprises an epoxy resin system, chosen for its superior char-forming characteristics, which is filled with silica and glass fibers for further enhancement of char stability and with phenolic microballoons for density control. This mixture is loaded into nylon-phenolic fiberglass honeycomb for further reinforcement and to facilitate fabrication of monolithic heat shield structures."

6. MATERIALS 7 AND 11

These materials are made by the Martin Company, Baltimore, for the Air Force PRIME Project. Test data¹ for the material are classified and are reported separately (see Ref. 3-1). The thermal protection system for the PRIME vehicle and most of the pertinent ablation materials properties are reported in Ref. 2-2.

¹For those desiring to obtain these data, requests should be made to the Air Force Space Systems Division, SSTR, Los Angeles Air Force Station.

7. MATERIAL 8

"THERMO-LAG T-500-111-H'C is a composite, honeycomb reinforced, subliming, ablative heat shield material manufactured by Emerson Electric Company. The ablative material is composed of an inorganic salt, subliming at approximately 530°F, an organic binder system, and additives for density control and for improvement of the chemical resistance and mechanical strength of the char resulting from pyrolysis."

"The honeycomb reinforcing material is composed of fiberglass cloth impregnated and coated with mixed nylon and phenolic resins. The honeycomb has an approximate density of 2.5 lb/ft³ and a cell size of 0.375 in. The density of the composite, reinforced material is approximately 35 lb/ft³."

8. MATERIAL 9

"The NASA Langley elastomeric material specimens (Purple Blend) consists of:

GE LTV-602 silicone resin	68.5%
GE SF-69 dimethyl oil	4.5%
GE SRC-04 catalyst	0.5%*
Union Carbide BJO-0930, phenolic microballoons	13.5%
Emerson and Cumming, Inc., Eccospheres (SI grade)	10.0%
Johns-Manville, Inc., 5 μ diam, 1/4 in. long, Microquartz fibers	3.5%

*Percent by weight of silicone resin

The densities of the specimens tested ranged from 32.4 to 32.9 lb/ft³."

9. MATERIAL 10

"The NASA/Langley low density phenolic nylon has the following composition:

Union Carbide BRP-5544, medium flow phenolic resin	25%
Union Carbide BJO-0930, phenolic microballoons	25%
Dupont Zytel 103 nylon, processed to 80 mesh power	50%

The density of the specimens tested was 32.6 lb/ft³."

C. SAMPLE PREPARATION

Generally, the materials described above were received in the form of 12 in. x 12 in. x 12 in. thick slabs, from which were machined 2 in. diam cylindrical specimens 2 in. long. The model size was chosen to be consistent with one-dimensional heat flow and minimum temperature conduction error for isothermal thermocouples installed in these materials.

D. TEST PROCEDURES

A 1/8 in. thick epoxy fiberglass sleeve was placed around each sample to minimize side heating and to keep the hot face in compression. The sleeve extended to within 1/2 in. of the specimen hot face. After the first three runs, the sleeve was made flush with the hot face because the honeycomb expanded more than expected, pulled away from the low density filler, and opened hot gas paths to the thermocouple junctions and to the interior of the specimens. After the fifteenth test, the sleeves were moved back to 1/4 in. from the hot face as a compromise, since it was felt that surface recession was being influenced due to the lower recessions experienced by the thick sleeve.

After run 16, loose fiberglass wool was added to the inside of the specimen holder to block the radiation paths from the exposed metal model holder to the model rear face. Rear face thermocouple measurements were not meaningful for prior runs due to a reflected shock impinging on the metal holder around the model base diameter. A button of epoxy resin was also added to the rear face to block potential gas paths through the sample.

At the end of the twenty-fourth test, refracil phenolic sleeving approximately 1/16 in. thick was used in place of the epoxy fiberglass in an attempt to achieve a better balance of the surface recessions of the retaining sleeve and the test material. The refracil phenolic sleeving, however, became incandescent during subsequent tests.

The program was halted temporarily after run 34 to evaluate test procedures and data collected to that time. Examination of the test movies revealed the shock attachment at the base of the brass sample holder, thus







explaining the anomalous rear face thermocouple measurements prior to run 34. Tests from number 35 on, therefore, used four layers of 1/16 in. asbestos tape fastened with fine nichrome wire loops around the outside diameter of the model holder. After test 43, epoxy fiberglass sleeving material was again used on the outside diameter which was also wrapped with asbestos and for awhile with a separate conical wrap, and then (after test 77) with one continuous wide wrap, always keeping the fiberglass sleeve 1/4 in. back from the hot face. Since the asbestos wrapping was included in the specimen weight and it ablated at the higher heat fluxes, the weight loss measurements were not used in the evaluation.

Generally, the criterion for the end of a test was when the specimen receded 1/2 in., when the 1 in. thermocouples read 500°F, or when 10 min elapsed, whichever came first. At the 20 and 60 Btu/ft² sec heat fluxes there was little recession, and one of the latter two were used.

In a typical test, the procedure used was as follows:

1. Measure specimen diameter with micrometer and the length with height gage.
2. Bond fiberglass retaining sleeve to outside diameter with silastic adhesive.
3. Cover rear face of specimen with epoxy and cure at 230°F.
4. Wrap thermocouple transitions (stainless sheathed to braided lead wire) in fiberglass rovings and insert into holder and place detent pins through holder into specimen.
5. Wrap specimen and holder with 4 in. wide asbestos tape and bind with 0.020 in. nichrome wire.
6. Weigh and photograph specimen-holder assembly.
7. Break vacuum, open tunnel chamber, and pull thermocouple leads through arc tunnel model support sting, attach leads to recording potentiometer and mount specimen holder in sting (Figs. 2-1 and 2-2).
8. Set spacing between specimen hot face and plasma generator nozzle exit face to 1-5/8 in. Close tunnel chamber and evacuate.
9. Photograph title onto motion picture film of model sequence.
10. Focus optical pyrometer and motion picture camera on specimen hot face. Set camera to photograph at 12 pps.

Table 2-2. Calibration Results

q Range, Btu/ ft ² sec	Test No.	Model Stagnation Pressure, atm	H/RT ₀	Q Calc, H/RT ₀	Centerline q			Aerospace Cal.			Calorimeter Position Facing Flow
					Q Calc, H/RT ₀	Corr, 5/8 Hem	Aerospace, Martin, q _B 2.0 F.F.	q _A	q _C	q _E	
20	7	0.0024	240	190	25.0	23.3	26.4	16.1	19.0	19.0	
60	4	0.0053	307	341	66.9	70.5	81.7	58.0	62.6	58.4	
90	9	0.0090	300	389	99.3	94.5	--	100.8	93.8	76.5	
120	2	0.028	298	286	128.0	122.0	--	123.0	126.0	111.0	
	4	0.027	289	286	128.0	124.0	--	132.0	128.0	116.0	
150	6	0.028	311	351	160.0	151.0	177.0	160.0	160.0	160.0	

11. Lower the specimen out of the plasma flow field with the sting actuator.
12. Turn on cooling water to specimen holder.
13. Start arc flow with argon, switch to nitrogen, and then add oxygen to mix downstream. Adjust power and mass flow settings.
14. Gimbal in the 5/8 in. hemispherical, water-cooled calorimeter, measure and record temperature rise for heat flux, then gimbal in pitot probe, measure and record model stagnation pressure. Record upstream nozzle stagnation and nozzle exit static pressure.
15. Place model in plasma flow for 10 min, 1/2 in. recession or 500°F at 1 in. thermocouple location, whichever comes first, then terminate arc flow.
16. Continue to record thermocouple data for 15 to 20 sec after arc termination.
17. Shut down all apparatus; examine records.
18. Open tunnel, remove specimen, photograph, weigh, and measure.

On arrival at Aerospace, specimens were split on a band saw, blown free of debris, and photographed in black and white and color. Samples were taken for X-ray diffraction, chemical, and char zone analysis.

E. CALIBRATION

For jet calibration purposes, three variables, model stagnation pressure, stream enthalpy, and cold-wall calorimeter heat flux, were investigated. All probes and calorimeters were placed 1.625 in. downstream of the nozzle exit and could be rapidly moved into the flow.

1. MODEL IMPACT PRESSURE

Radial surveys of the jet were made with a 0.50 in. diam flat-face impact probe. It was found that pressure variation over the 2 in. diam model area varied less than 5% of the centerline value. Table 2-2 lists model impact pressure P_{oy} for various calibration points.

2. STREAM ENTHALPY

Average jet enthalpy was determined from an energy balance on the arc system. The various cooling water losses were subtracted from total power

input to the arc to give net energy in the gas stream. This value together with air mass flow rate through the nozzle allows determination of average bulk enthalpy of the exit gas stream.

Since it is generally recognized that enthalpy gradients exist in arc jet flows, the local centerline enthalpy was measured for comparison with the average bulk value. This may be calculated from the measured centerline heat flux and impact pressure. The following simplified correlation (for Lewis number = 1.0) from Ref. 3-2 may be used for equilibrium heat transfer to a hemispherical calorimeter:

$$q \left(\frac{R}{P_{oy}} \right)^{1/2} = 0.0417(h_{oy} - h_w) \quad (2-1)$$

where q is the heat transfer rate in Btu/ft²sec, R is the nose radius in feet, P_{oy} is the model stagnation pressure in atmospheres, and h_{oy} and h_w are the local stagnation and wall enthalpy values, respectively, in Btu/lb. Over the range of interest of this study, Eq. (2-1) agrees to within a few percent with the more detailed equations of Ref. 2-4.

The centerline jet enthalpy shown in Table 2-2 was calculated Eq. (2-1) from heat flux data obtained with the 5/8 in. diam hemispherical calorimeter described in the following section. This enthalpy is presented for reference only as it can be shown (Ref. 2-5) that a measured centerline enthalpy which is lower than that of the true stagnation value can be expected due to non-equilibrium effects in the stagnation point boundary layer. Possible non-equilibrium effects encountered during calibration and testing are being investigated in detail.

3. CALORIMETRY

In addition to the data obtained from the 5/8 in. hemispherical calorimeter, a 2 in. diam flat faced model developed at Aerospace was used to obtain cold wall heat flux levels at the exact model location. Subsequently, the calibration points were also investigated using a set of calorimeters from

the Martin Company. All calorimeters had visibly clean copper surfaces in contact with the flow.

The 5/8 in. hemispherical calorimeter was a water-cooled, steady-state design (Ref. 2-6). This device was used initially to roughly set the test point for a more refined investigation with the Aerospace and Martin calorimeters. Heat flux data from the 5/8 in. calorimeter were corrected to flat face geometry using the 0.55 factor recommended in Ref. 2-7. Including the additional square root correction from 5/8 to 2 in. diam (Eq. 1) gives a combined factor of 0.307 to correct the measured heat flux for the 5/8 in. hemisphere to 2 in. diam flat faced geometry. This corrected value is shown in Table 2-2 for the 5/8 in. calorimeter.

Test points were investigated in more detail with the 2 in. diam heat flux profile calorimeter developed at Aerospace. This unit (Fig. 2-3) consists of a 2 in. diam copper face plate into which are inserted five copper slugs of 0.250 in. diam frontal dimension. The slugs were insulated with thin Delrin spacers in the rear and with high temperature cement in the front surface groove. No cooling was provided for this calorimeter. The slugs each weighed 2.0 g and were fitted with iron-constantan thermocouples at the rear, giving a transient response of

$$\dot{q} = 1.18 \frac{dT}{d\tau} \quad (2-2)$$

with \dot{q} in Btu/ft²sec, dT in °F, and $d\tau$ in sec. The maximum temperature at the rear of the slugs was limited to about 250°F due to the low temperature Delrin insulation. Also calorimeter surface temperatures were kept low to reduce possible heat losses by conduction to the copper face plate. The slugs and face plate are sized to give approximately the same temperature rise and thus aid in reducing slug heat loss by conduction. The analysis of Ref. 2-8 shows that approximately 0.3 sec was required for starting transients after the calorimeter had been snapped into the flow. The curve of temperature vs time after this initial period is represented by a straight line

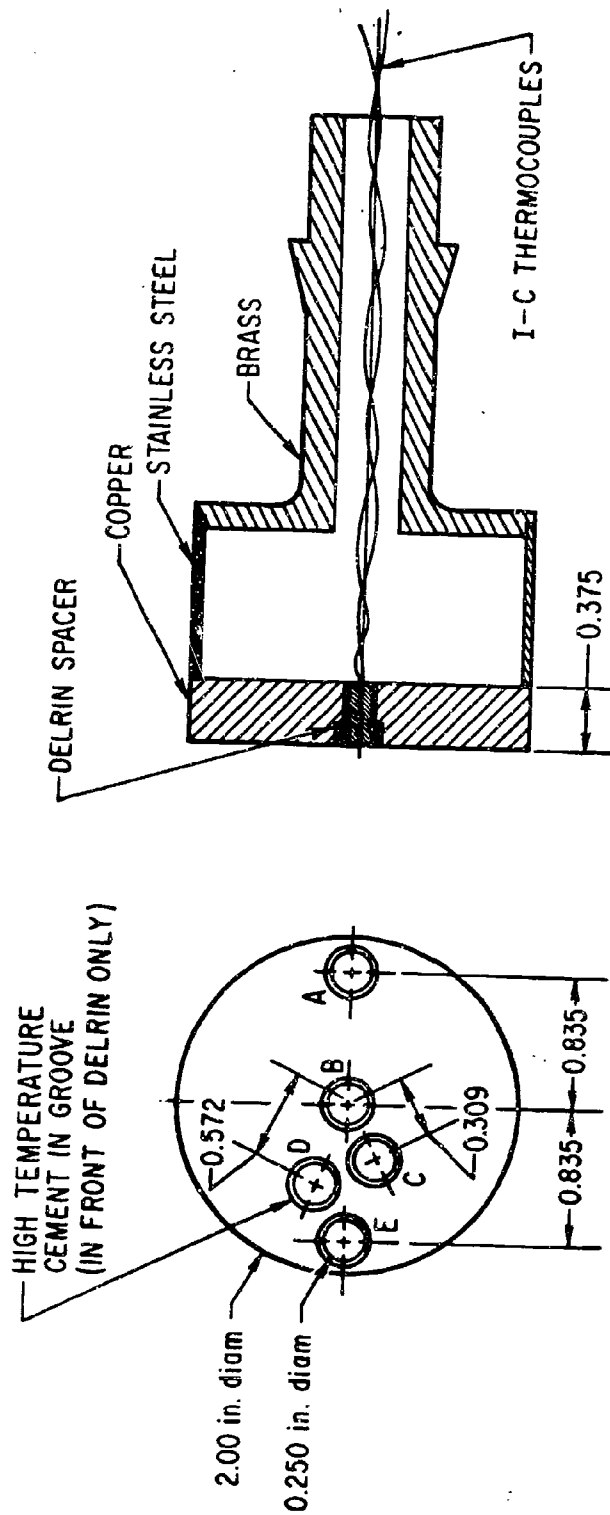


Fig. 2-3. Aerospace Calorimeter Construction

if no heat loss from the slug takes place. Table 2-2 allows comparison of the corrected 5/8 in. hemispherical heat flux with the 2 in. flat faced profiles. Close agreement exists between the hemispherical data and centerline heat flux (\dot{q}_B) on the flat faced unit. The slope of the temperature vs time curve was obtained from a recorder chart for use in Eq. (2-2). Table 2-2 also shows heat flux profiles across the 2 in. flat faced calorimeter. It is felt that the final values shown represent the flattest possible profile with the existing nozzle. Heat flux profile values on various radii (see Fig. 2-3 for slug locations) were obtained by rotating the Aerospace calorimeter, as shown in Table 2-2. Note that the heat flux to element D is not tabulated as it was read on a separate recorder which was later found to contain a faulty circuit. Both calorimeters were used during a single arc run by manually rotating the steady state unit into the stream and then later in the same run pneumatically snapping-in the transient device. Due to the close agreement between the two calorimeters, it was decided to use the more conveniently operated hemispherical steady state unit with the impact probe for test point checking immediately before inserting an ablation model. All system inputs, such as electrical energy, gas and water flows, and test section pressure, were recorded during the calibration studies and duplicated for the ablation model runs.

Additional investigations were carried out at selected test points with several calorimeters from the Martin Company. These units were constructed with 0.250 in. diam copper slugs inserted in a 2 in. diam phenolic asbestos body. Designs with either one centerline element or eight slugs located as shown in Fig. 2-4 were used. The front face slugs had a transient response of

$$q = 1.07 \frac{dT}{dT} \quad (2-3)$$

using units identical to Eq. (2-2). Table 2-2 lists the measured centerline heat flux values for comparison with the other calorimeters, and the data show

that close agreement was obtained. The greatest deviations are approximately 15 to 20% high for the Martin calorimeter at the 60 Btu/ft² sec test point. Side heating rates were investigated using the eight element calorimeter shown in Fig. 2-4. It was found that the side heat flux ranged in the order of 1/8 to 1/10 of the stagnation point values.

REFERENCES

- 2-1. C. M. Dolan, Study for Development of Elastomeric Thermal Shield Materials, NASA CR-186 (March 1965), p. 6-2.
- 2-2. J. Slaughter, J. Meltzer, and D. V. Sallis, "PRIME Vehicle Heat Protection System," Paper presented at the Tenth Symposium on Space and Ballistic Missile Technology, San Diego, Calif., 4-6 August 1965 (C).
- 2-3. N. K. Hiester and C. F. Clark, Relative Operating Capabilities of Selected Electric-Arc Reentry Environment Simulators, Stanford Research Institute Report on NASA Contract No. NASr-49 (15), Menlo Park, Calif. (1964).
- 2-4. C. H. Lewis and E. G. Burgess, III, Charts of Sphere Stagnation Heat-Transfer Rate in Air and Nitrogen at High Temperatures, AEDC-TDR-63-139, Arnold Engineering Development Center, Arnold Air Force Station, Tenn. (July 1963).
- 2-5. P. M. Chung and S. W. Liu, "Simultaneous Gas-Phase and Surface Atom Recombination for Stagnation Boundary Layer," AIAA Journal 1 (4), 929 (April 1964).
- 2-6. R. D. Buhler, D. Christensen, and S. Grindle, Effects of Hyperthermal Conditions on Plastic Ablation Materials, ASD TR 61-304, Plasmadyne Corporation, Santa Ana, Calif. (1961), p. 37.
- 2-7. W. E. Stoney and J. J. Markley, Heat Transfer and Pressure Measurements on Flat Faced Cylinders at a Mach Number of 2, NACA TN 4300 (July 1958).
- 2-8. R. H. Kirchoff, "Calorimetric Heating-Rate Probe for Maximum-Response-Time Interval," AIAA Journal, 2 (5), 966 (May 1964).

PART 3. AEROTHERMODYNAMIC RESULTS

I. INTRODUCTION

The preliminary consideration of the feasibility of ablative thermal protection systems for lifting reentry vehicles requires that some idea be gained of the general regimes of recession and thermal response to be expected from the currently available materials. Under the PRIME program, the Air Force is investigating the feasibility of such systems. To obtain comparative information on materials, it is convenient to test them under simulated re-entry heating conditions at one time in one arc tunnel facility to minimize any spurious differences that might otherwise occur. Aerospace Corporation and AFML-Wright Field have jointly conducted tests at the Giannini Scientific Corporation, Santa Ana, California. The results of those tests, in particular, the aerothermodynamic results, including recession and temperature response, are reported here.

The raw-data results of these tests are reported in Ref. 3-1. As specified in Part 1 the specimens of materials 2A and 2C (Lockheat) were not designed for use at heat fluxes over $50 \text{ Btu/ft}^2 \text{ sec}$, although this is not necessarily a general limitation according to the supplier. These materials did not perform satisfactorily at the higher heat flux conditions, and accordingly only the test results at the lowest heat flux are presented.

Sections II - IV describe the results of the thermal test series (89 tests), in which flat faced cylindrical specimens of 2 in. diam and 2 in. length were heated at one end with a supersonic air arc flow. Thermal response analyses and recession analyses are discussed in Sections V and VI. Section VII describes the results of the shear test series (9 tests), in which specimens were inserted flush with one face of a 15 deg half-angle wedge model facing a supersonic air arc flow.

The heat flux levels chosen for the thermal test series are representative of levels which would be encountered on the major body surfaces of an

ablative lifting re-entry vehicle, as currently envisioned. Heat fluxes up to $150 \text{ Btu/ft}^2 \text{ sec}$ were emphasized because of potential problems with recession during peak heating near the forward portion of the body. Air enthalpy levels ranged from 8150 Btu/lb at the lowest heat flux to 10,550 at the highest heat flux. Model stagnation pressures correspondingly ranged between 0.0024 and 0.028 atm. Test duration was typically 600 sec at the two lower heat flux levels and somewhat less at higher heat fluxes.

It is recognized that these results are preliminary and do not constitute an unqualified and final characterization of the materials tested. As discussed in the following sections, certain aspects of the tests were unsatisfactory. The shear test results are unacceptable because of severe damage to the specimen mounting ring in all tests. Rear-face temperatures in the thermal test series were invalidated in some tests because the specimen holder was inadequately insulated. However, the front surface temperature and recession results and the internal (1 in. depth) temperature results are believed to be valid and comparable in most cases. These results furnish an initial comparison of ablation performance for these materials.

II. RECESSION RATE

An effective recession rate for the thermal tests was calculated from the length change of the specimen and the test duration. In cases where the specimen front surface remained flat, the final length was measured at the specimen centerline (which was typically the point of maximum recession). Two factors caused a dishing of the front surface: first, the distribution of convective heat flux usually involved a maximum near the centerline (Part 2); and second, the ablative shroud around each specimen often receded less than the specimen at the front surface. The effect of dishing on the convective heat flux was not evaluated.

Figure 3-1 (bar graph) shows the recession rate calculated for all tests, for each of the five heat flux levels. Except for those with a plus sign above the bar, all data are for length loss during the test. A plus sign indicates that the specimen expanded; this condition occurred for many materials at the two lower heat flux levels. Each bar is designated with two numbers: the upper one indicating the model (or test) number, and the lower one, the material identification number. The test numbers correspond to those of Ref. 3-1.

III. TEMPERATURE MEASUREMENTS

A. FRONT-SURFACE TEMPERATURE

The front-surface brightness temperature of each specimen undergoing a test was measured using a manual disappearing-filament pyrometer, taking readings every 30 sec. The temperature reached a steady level within the first 30 sec and remained constant throughout the test.

Figure 3-2 shows the brightness temperature level achieved in each thermal test, summarized at each heat flux level. For reference, the radiation equilibrium temperature for a surface of 0.85 emissivity is shown for each heat flux. This radiation equilibrium temperature was calculated using a heat balance between convection and radiation, where the convection was scaled from the calorimeter values to account for the actual enthalpy difference across the boundary layer. The emissivity value of 0.85 was chosen as typical of charred ablator surfaces.

A small positive correction results from a conversion from brightness temperature to actual temperature for a surface of reasonably high emissivity. This is on the order of 50°R , as an example, for a surface of 0.85 emissivity at a brightness temperature of 3500°R . This correction has not been applied to these results because of a lack of emissivity data, but it is evident from Fig. 3-2 that the correction cannot be very large as most data approached the radiation equilibrium temperature shown.

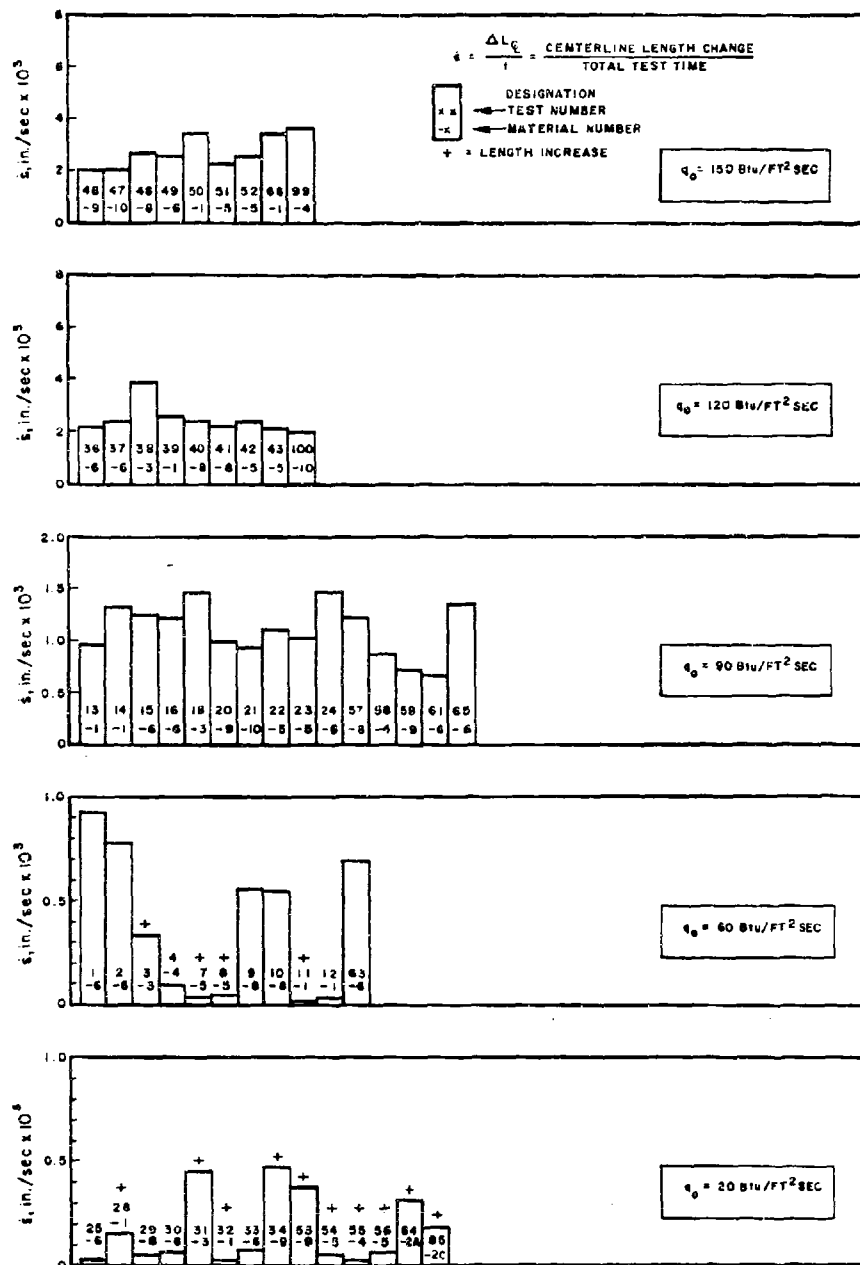


Fig. 3-1. Front Surface Recession Rate

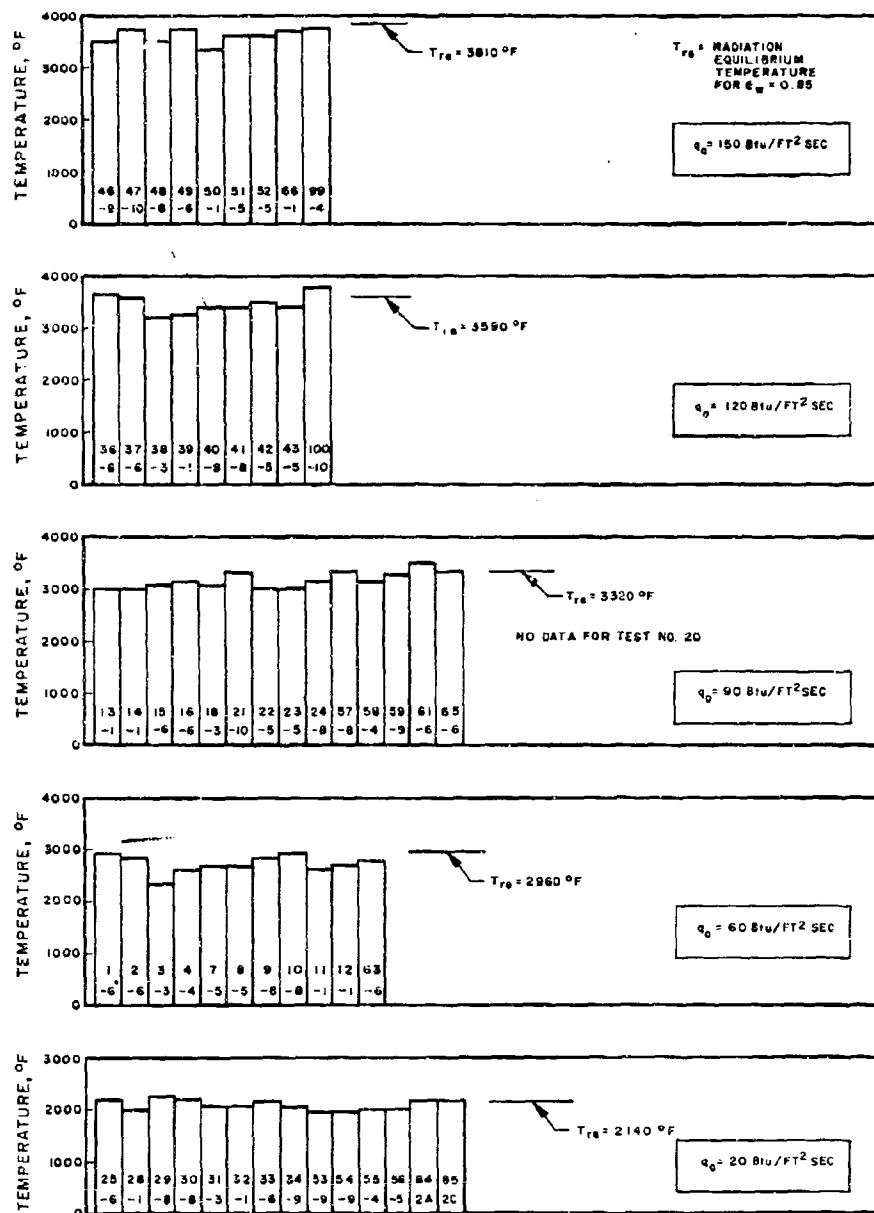


Fig. 3-2. Front Surface Brightness Temperature

The pyrometer view of the ablator surface was direct, at an angle of about 45 deg to the surface, eliminating the need for any substantial correction for geometry or reflection.

At the conclusion of this testing program some comparison tests were run in the Aerospace Corporation arc facility, which indicated somewhat lower surface temperatures and recession rates, using an elastomeric material at 90 and 150 Btu/ft²sec nominal heat flux levels. These differences are believed to be the result of a partly noncatalytic characteristic of the charred front surface of that material combined with different nonequilibrium gas-phase conditions in the test flow. In all cases, the nominal heat fluxes referred to are those measured using a clean copper calorimeter and are considered to be close to the catalytic value. The surface temperatures reported here therefore may not be generally applicable; detailed testing of each material is required to determine the surface temperature for specific conditions.

B. REAR-FACE TEMPERATURE

The rear-face temperature was measured using a thermocouple attached to a small copper disk which was attached to the rear face of the specimen at the center. The disk, 0.5 in. diam and 0.030 in. thick, was attached with epoxy resin. Early difficulties with excessive rear-face temperatures led to the application of additional epoxy resin over the entire rear face. The additional resin was about 0.075 in. thick and covered the central disk and thermocouple, and it sealed the face from a possible diffusion of hot gas in either direction.

Measured rear-face temperatures are shown for each heat flux level in Fig. 3-3 - 3-6. From these figures it is evident that tests 1 through 34 involved a spurious heating of the rear face. After test 34, several layers of asbestos paper were wrapped around the metal specimen holder, which controlled the rear-face heating to a much lower level. Apparently the external convective heating was sufficient to heat the holder, which radiated heat to the specimen rear face in the early tests. It is shown later that the rear-face temperature response even in tests after 34 is not entirely free of

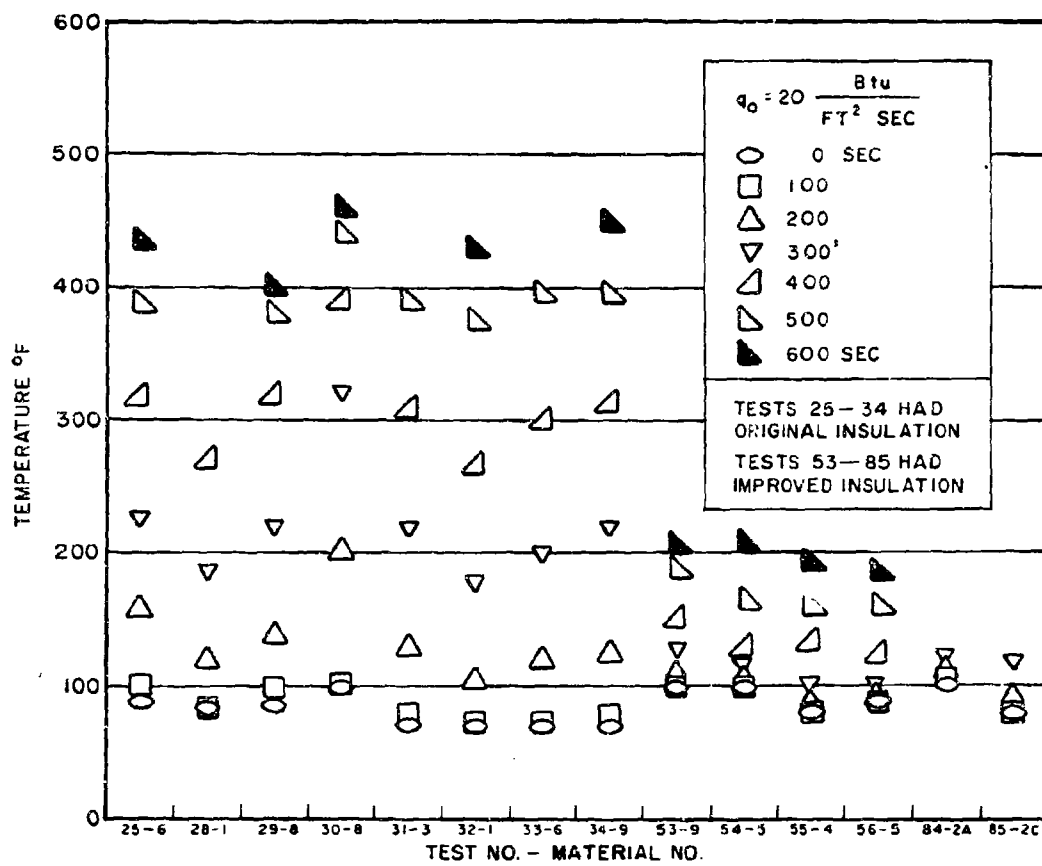


Fig. 3-3. Rear-Face Temperature Response at $q_0 = 20 \text{ Btu/ft}^2 \text{ sec}$

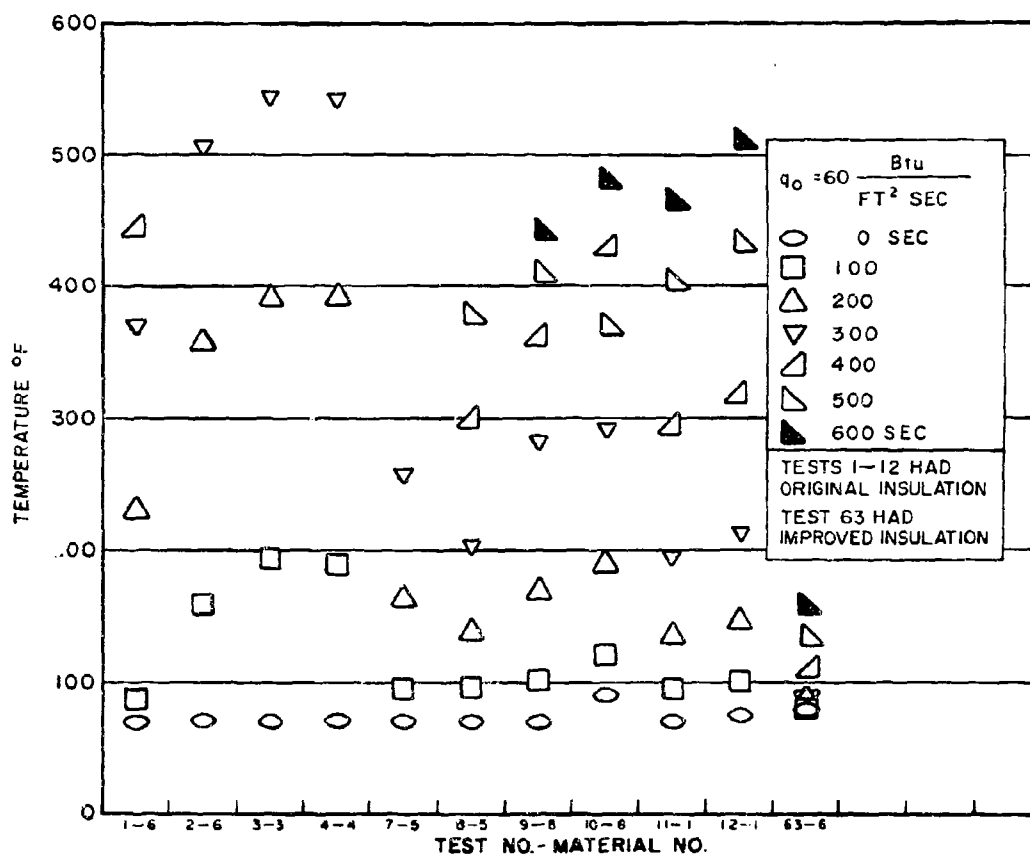


Fig. 3-4. Rear-Face Temperature Response at $q_o = 60 \text{ Btu/ft}^2 \text{ sec}$

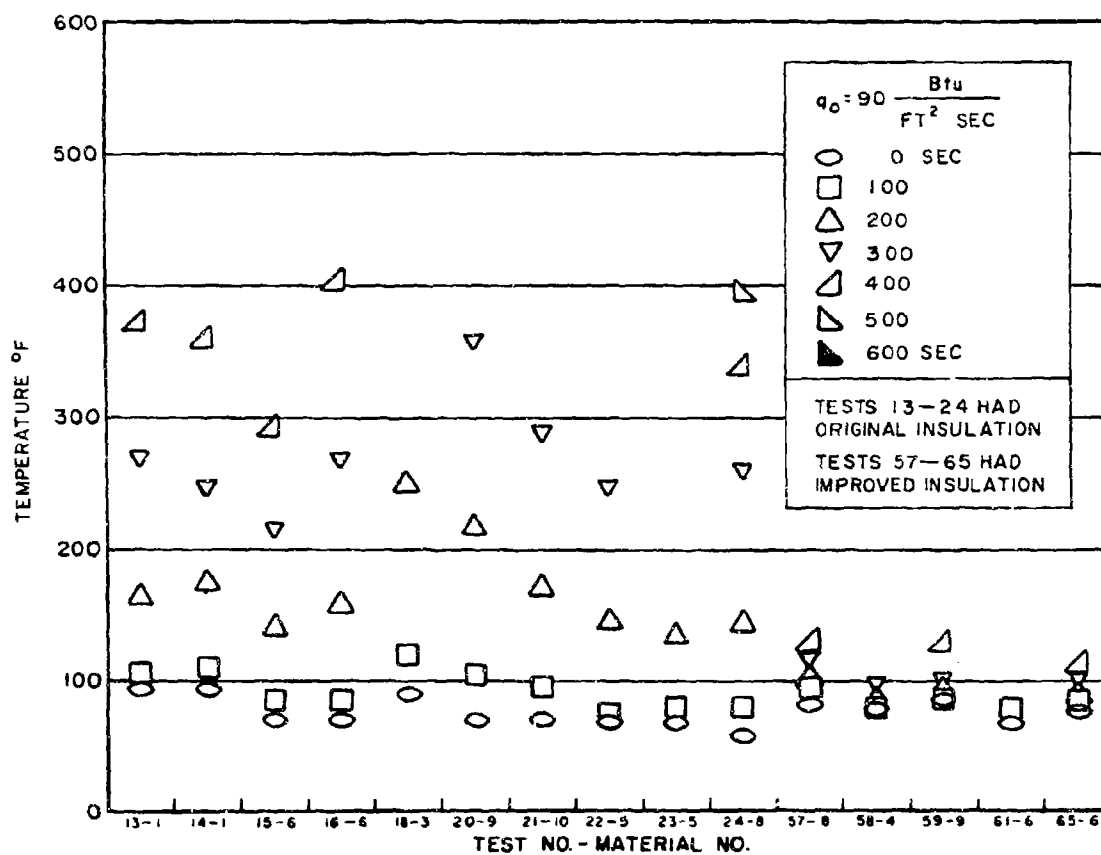


Fig. 3-5. Rear-Face Temperature Response at $q_o = 90 \text{ Btu/ft}^2 \text{ sec}$

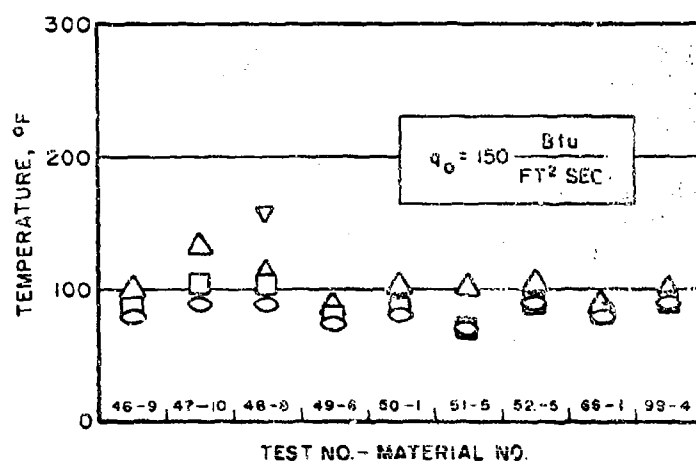
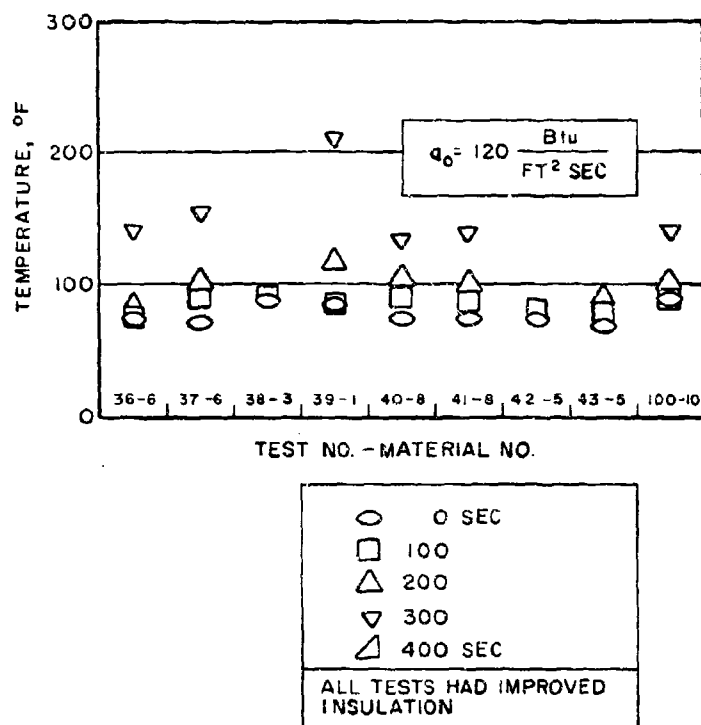


Fig. 3-6. Rear-Face Temperature Response at $q_0 = 120$ and $150 \text{ Btu/ft}^2\text{sec}$

spurious heating effects. Such effects were apparently small enough, however, that they are probably inseparable from other effects, such as those of three-dimensional conduction within the specimen.

For these reasons, it is recommended that attention be turned to the internal (1 in. depth) temperature response for a better picture of the comparative thermal conduction properties of these materials.

C. INTERNAL TEMPERATURES

Specimen internal temperature was measured at the 1 in. depth using a redundant pair of thermocouples at opposed positions with each junction located 1/8 in. from the centerline. Each thermocouple consisted of chromel-alumel wires inside a stainless-steel sheath of 0.020 o.d., with magnesia internal insulation. The junction was formed by welding, leaving 0.050 in. of exposed wire between the junction and the sheath. Each thermocouple was inserted into a 0.022 in. diam radial hole leading toward the specimen axis, and the junction was lightly pressed to the hole bottom. The thermocouple was then bent axially into a groove along the peripheral surface and let into the cavity at the rear of the specimen where a transition was made to flexible chromel-alumel lead wires.

A sizable fraction of the tests showed conflicting results, comparing the two thermocouple readings at the 1 in. depth. Typically, one of the thermocouples would appear to indicate an erroneously high temperature by several hundred degrees. It is believed that in spite of the relatively long immersion depth (L to D of about 40), heat conduction from the hot specimen periphery must have occurred in the thermocouple sheath to cause this high reading. Assuming this was the case, the lower of the two readings is taken as the significant value. The measurements, interpreted in this way, are shown for all tests in Figs. 3-7 - 3-9. If one thermocouple reading is erroneous because of sheath conduction effects perhaps the other thermocouple could also be in error to a lesser degree. This possibility was examined in data from repeated tests at a given heat flux level. It may be seen that in most cases the agreement is reasonably good, lending credibility to the assumption that the lower reading taken here is reasonably free of conduction errors.

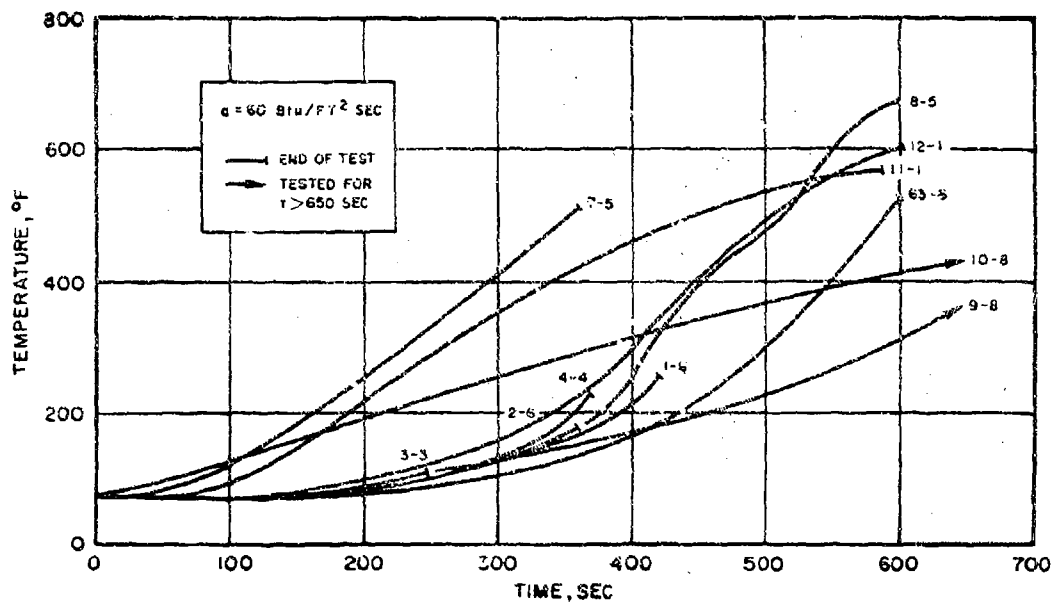
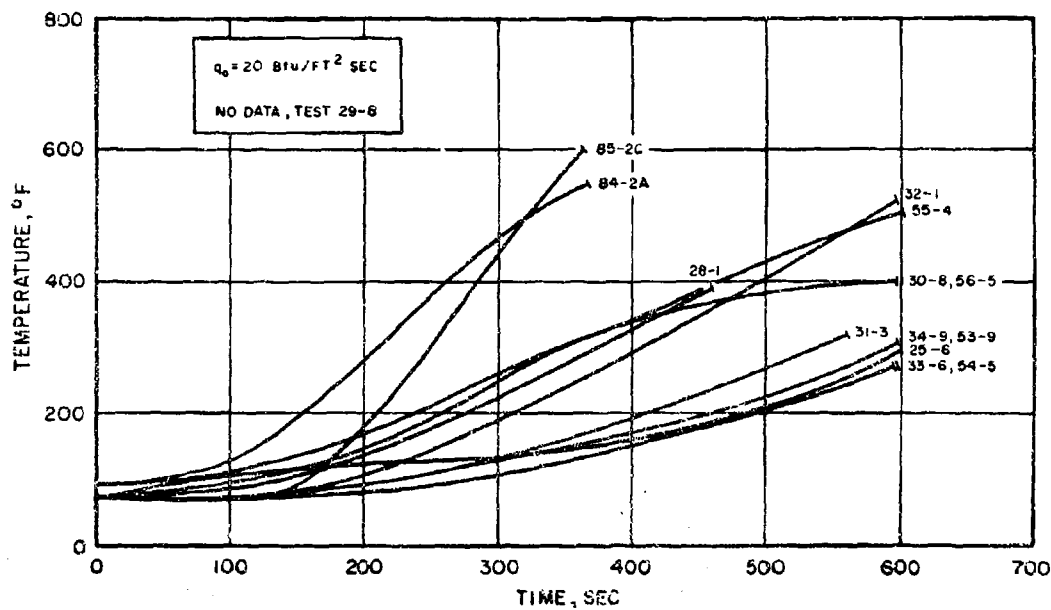


Fig. 3-7. Temperature Response at 1 in. Depth, $q_0 = 20$ and $60 \text{ Btu/ft}^2 \text{ sec}$

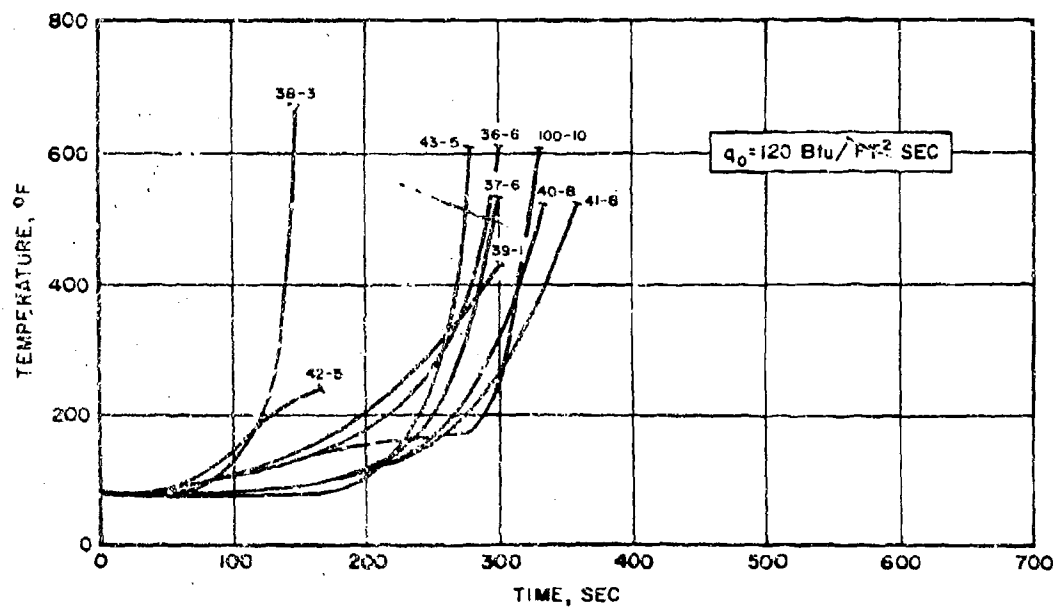
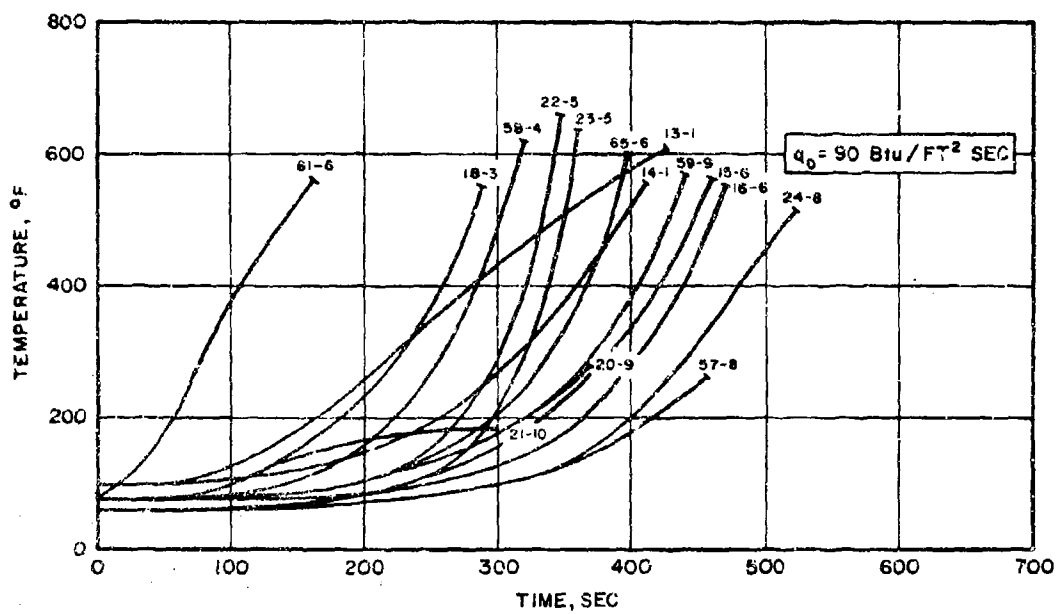


Fig. 3-8 Temperature Response at 1 in. Depth, q_0 90 and 120 Btu/ft²sec

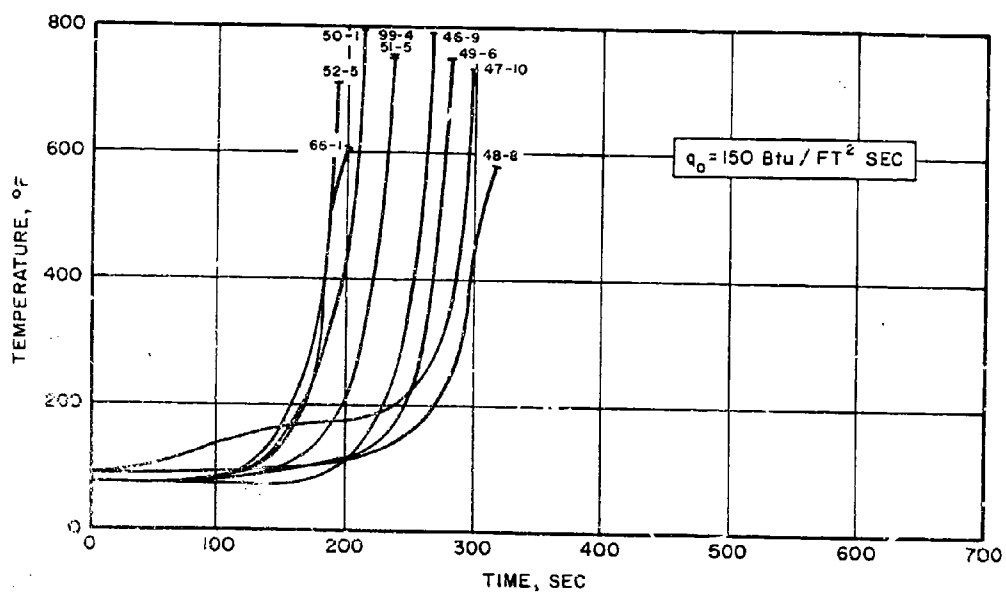


Fig. 3-9. Temperature Response at 1 in. Depth, $q_0 = 150 \text{ Btu/ft}^2 \text{ sec}$

A close inspection of Figs. 3-7 - 3-9 reveals that a few tests produced internal temperature data (again using the lowest reading thermocouple) which appear erroneous. For example, referring to Fig. 3-8, the results for material 6 at $90 \text{ Btu/ft}^2 \text{ sec}$ indicate that test 61-6 produced an erroneous result. It is presumed that this and other such tests suffered thermocouple conduction errors, as described above, in both of the thermocouples at the 1 in. depth. Where the number of tests reported for a material at a given heat flux level is insufficient to identify such anomalous thermocouple behavior, it is recommended that reference be made to comparative performance at other heat flux levels.

IV. CHAR DEPTH MEASUREMENTS

Table 3-1 shows the post-run measurements of char thickness for all materials except 2A and 2C, which are not conventional ablators. In most cases the observable profile of the char-virgin interface was reasonably flat. The heated surface became dished in some of the tests where recession occurred, and to prevent ambiguity the char depth was measured at the centerline of each specimen.

V. THERMAL RESPONSE ANALYSIS

In order to rank the thermal performance of these ablation materials each material was compared with an idealized heat conductor. Since the thermal properties of ablative materials vary considerably computer analysis will be required to accurately predict flight performance. It is shown, however, that the temperature results obtained in these tests are characteristic of materials with reasonably constant thermal properties for the two lower heat flux levels. Surface recession at the higher heat fluxes prevents a straightforward conduction analysis.

Table 3-1. Char Thickness Measurements

Material No.	Heat Flux Level, Btu/ft ² sec				
	20	60	90	120	150
1	28-450-.400 32-597-.440	11-585-.810 12-675-.890	13-426-.370 14-105-.420	39-300-.220 --	50-210-.140 66-200-.170
3	31-552-.600	3-343-.650	18-285-.400	38-147-.100	--
4	55-599-.570	4-370-.720	58-314-.570	--	99-235-.320
5	54-598-.550 56-600-.580	7-360-.720 8-594-.840	22-345-.560 23-360-.630	42-169-.340 43-275-.460	51-233-.400 52-193-.400
6	25-652-.350 33-592-.470	1-420-.300 2-360-.320 63-601-.470	15-440-.400 16-470-.380 61-160-.350 65-400-.370	36-300-.230 37-297-.230 -- --	49-281-.250 -- -- --
8	29-600-.320 30-600-.270 57-453-.190	9-960-.450 10-975-.340	24-525-.220 --	40-332-.120 41-359-.170	48-315-.120 --
9	34-594-.540 53-599-.280	-- --	20-367-.520 59-460-.540	-- --	46-269-.200 --
10	--	--	21-360-.370	100-331-.315	47-298-.350

NOTES: The numbers separated by hyphens represent test no., test time, and final char thickness. Test time is measured in seconds and thickness is given in inches. Char thickness is measured depth at specimen centerline from heated surface to point where coloration of material first becomes indistinguishable from virgin material after specimen has cooled.

Consider a slab of material of thickness L , infinite in extent normal to the thickness and at an initially uniform temperature t_i . At time $\theta = 0$ two surfaces of the plate are suddenly heated to a temperature t_1 and maintained at that temperature. Schneider (Ref. 3-2) shows that the internal temperature response of this plate is

$$\frac{t - t_1}{t_i - t_1} = \frac{4}{\pi} \sum_{n=1}^{\infty} \exp \left[-\left(\frac{n\pi}{2}\right)^2 \Theta \right] \sin \frac{n\pi}{L} x \quad ; \quad n = 1, 3, 5, \dots \quad (3-1)$$

where

t = temperature at position x (depth from either face)

$\Theta = \alpha \theta / \delta_1^2$, the Fourier modulus

$\alpha = k / \rho c_p$, the thermal diffusivity, ft^2/sec

θ = time, sec

$\delta_1 = L/2$, mid-plane depth, ft

Solutions of Eq. (4-1) are shown in Fig. 3-10 for X/L values of 0.5 and 0.75. Since the temperature distribution must be symmetrical about the midplane at depth δ_1 and the gradient must correspondingly vanish at δ_1 , this configuration is identical to that for an infinite plate of thickness δ_1 heated to temperature t_1 on one side and insulated on the other. Thus, if the ablation specimens in the tests suffered no side heating or cooling and no heat transfer at the rear face, their temperature response should be comparable to the infinite plate of half-thickness δ_1 .

It can be noted from Fig. 3-2 that all tests at a given heat flux level indicated almost identical values of apparent surface brightness temperature. Average surface temperatures were selected from the 20 and 60 heat flux results at 2075 and 2700°F, respectively. With the use of these surface temperatures and the average initial temperature of 80°F, theoretical temperature responses for the 1 in. depth were calculated using the solution of Fig. 3-10 for an X/L value of 0.75. The value of δ_1 was taken as 2 in. (which

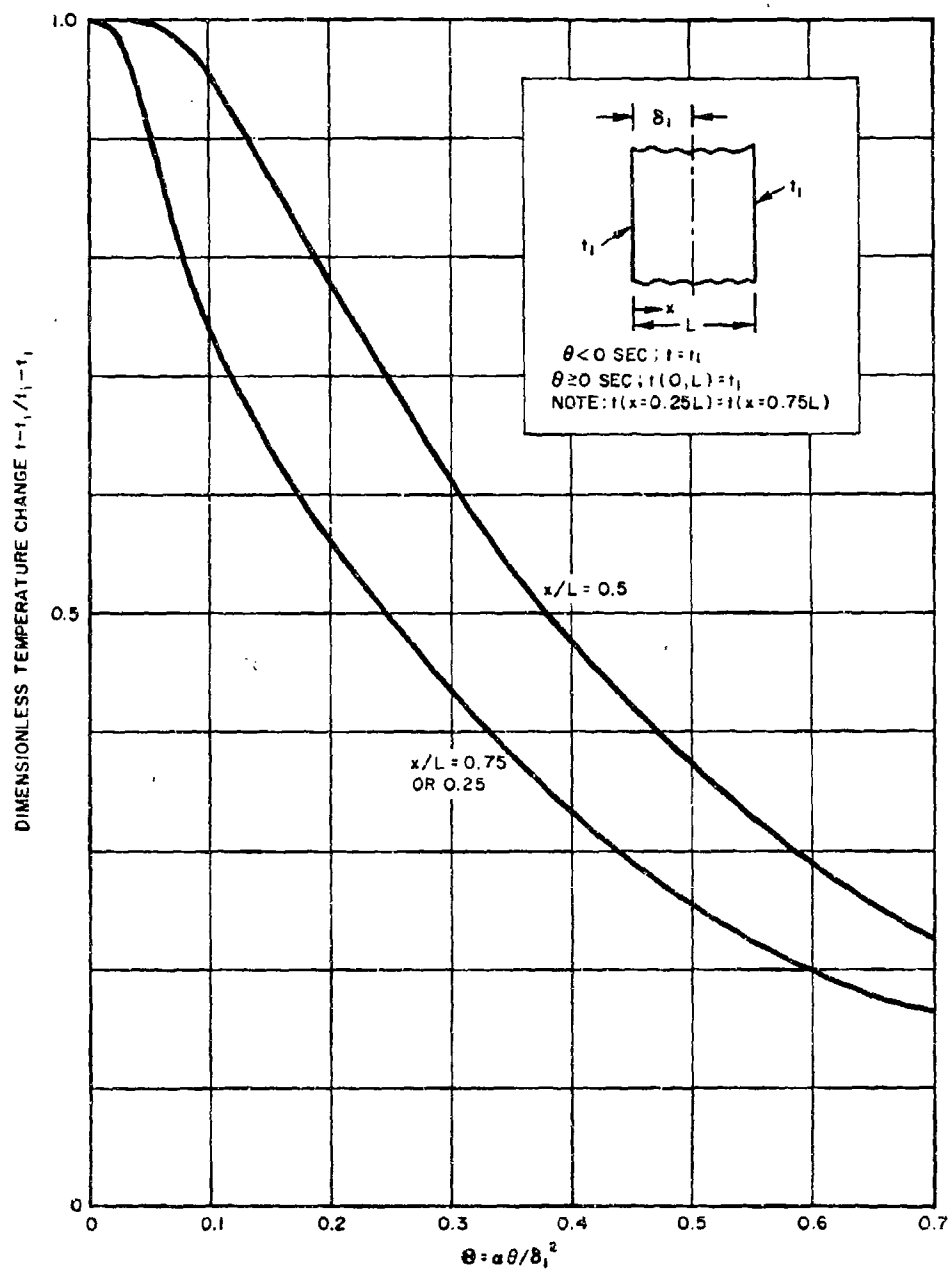


Fig. 3-10. Infinite Plate Conduction Solution

was the initial specimen thickness), and thermal diffusivity values from 1×10^{-6} to 7×10^{-6} ft²/sec were assumed. These results are shown in Fig. 3-11 superimposed on the experimental temperature response curves.

The comparisons made in Fig. 3-11 are worthy of study. They are helpful in identifying the following:

- a. Anomalous results.
- b. Scatter of data for a given material.
- c. Magnitude of the differences between materials.
- d. Time variations of apparent diffusivity.

It can be noted in Fig. 3-11 that there is a tendency for the effective thermal diffusivity to rise with time for most of the materials. It is known that as a typical ablator is converted to degraded material (or char) the thermal diffusivity rises steeply and also that diffusivity rises with increasing temperature. Therefore, it is remarkable that the effective diffusivity which can be deduced here remains as constant as is apparent. Two possible causes can be hypothesized for the apparent diffusivity behavior: first, the effects of depolymerization and gas diffusion tend to counteract the effect of increased conductivity in the charred region; second, the thickness of the charred region must be appreciable to cause a significant change in the apparent diffusivity for the entire thickness.

Side heating and rear-face heating have occurred to some extent in these tests; each would have the effect of increasing the apparent diffusivity with time. Therefore, it can be observed that in the absence of spurious heating the apparent diffusivity would remain even more constant than observed in Fig. 3-11. It can be seen from Figs. 3-3 and 3-4 that in the early tests (before No. 35) where excessive rear-face heating was observed an average (spurious) driving potential for heating at the 1 in. depth of about 10% of the primary (front-face temperature) potential existed. This implies that a positive 10% error existed in the (1 in. depth) temperature rise for those tests. Later tests, with a lower rear-face temperature rise, are shown to have been essentially free of that error.

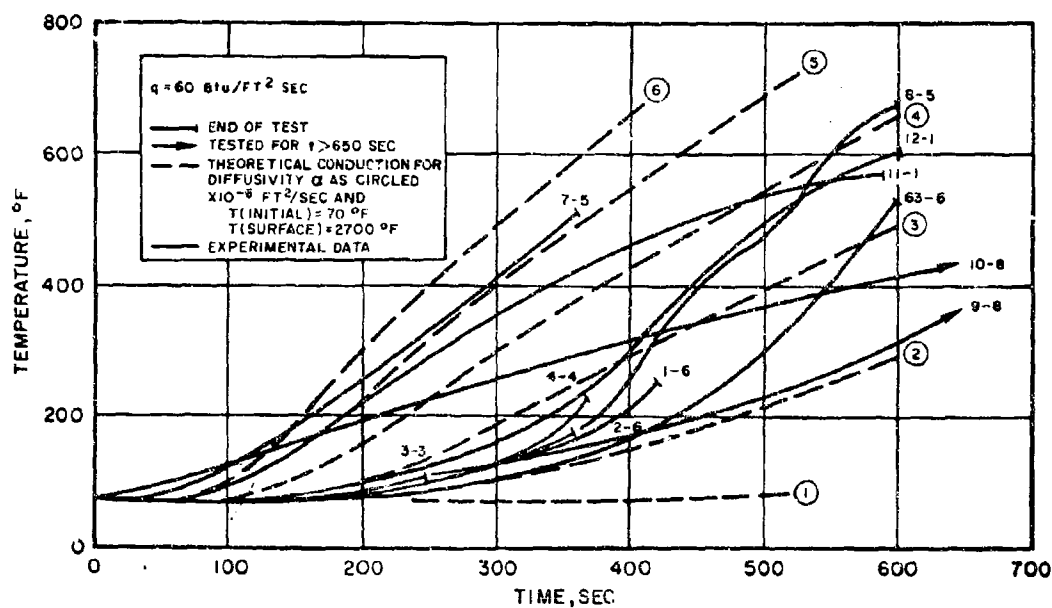
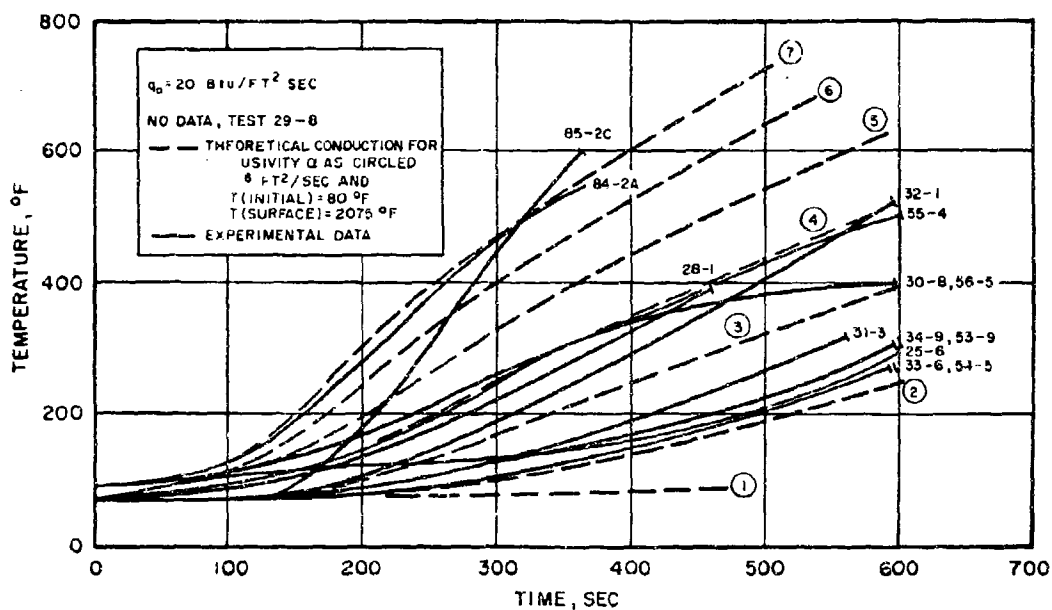


Fig. 3-11. Comparison of Thermal Response

An insulation efficiency E can be calculated from these results using the definition

$$E = \frac{q_o \theta}{\rho \delta}$$

where

q_o = cold wall heat flux, Btu/ft² sec

θ = time to a given temperature limit at a specified depth δ , sec

ρ = material density (initial), lbm/ft³

δ = thickness or depth, ft

E = insulation efficiency, Btu/lbm

This parameter is discussed in Ref. 3-4; it is indicated that the insulation efficiency E is useful for evaluating relative performance of materials but is insufficient for heat shield design purposes. It is seen that even for relative performance comparisons care must be exercised in calculating E since it is not strictly applicable for arbitrary times and thicknesses. As these insulating ablators are investigated further, it will be desirable to devise a more generally applicable figure of merit. Several alternative definitions of temperature limits and depths exist which will yield different values of E :

- a. E_a - Limiting temperature at the rear face of an ablator of thickness δ_1 , insulated rear face.
- b. E_b - Limiting temperature at the rear face of an ablator of thickness δ_1 , with an attached substrate of specified heat capacity and at the temperature of the ablator rear face.
- c. E_c - Limiting temperature at a depth δ_1 in an ablator of thickness δ_2 , with an insulated rear face.

The simplest alternative, although not the best, for evaluation of the present tests is (c). This is ambiguous because the total thickness δ_2 plays a role in the temperature rise at depth δ_1 , even though δ_1 is the only thickness used in the calculation of E . Since these materials indicate almost

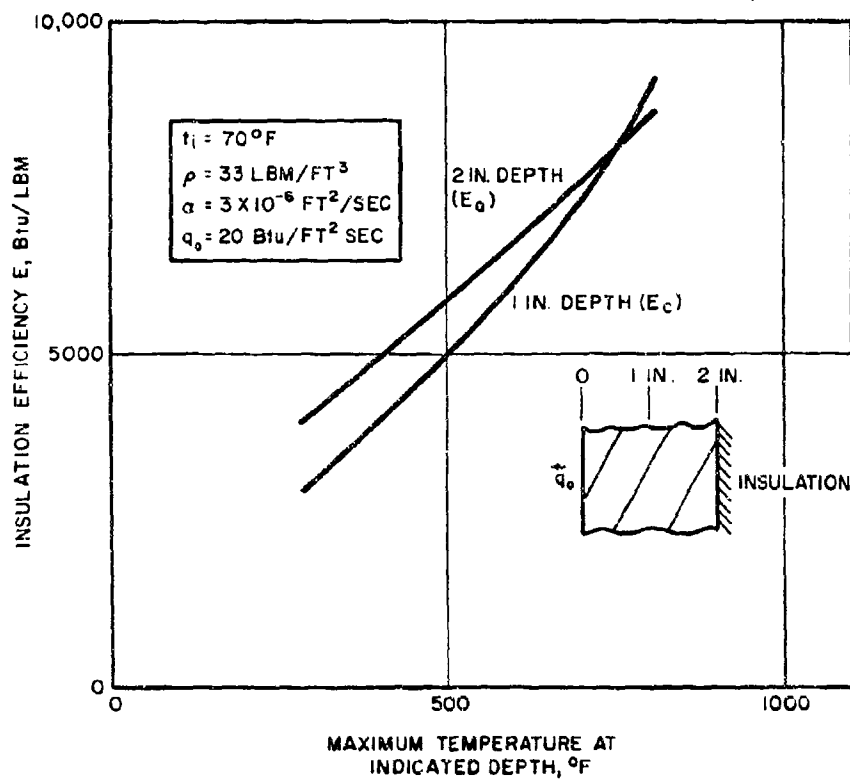


Fig. 3-12. Theoretical Error in E Based on Half-Depth Temperature

constant values of apparent diffusivity, it is a simple matter to demonstrate the error in E caused by the use of (c) compared to the unambiguous value obtained with (a). The error shown in Fig. 3-12 was obtained using the curves in Fig. 3-10 and typical material property values for the case of $q_o = 20$ Btu/ft²sec. For a maximum rear-face temperature of 300°F (230°F rise) a 25.7% negative error results.

In view of the error involved in forming an efficiency E_c based directly on the temperature measurement at 1 in. depth, a theoretical extension was made to permit the calculation of E_a . This was done by using the apparent diffusivity demonstrated at the 1 in. depth and the curves of Fig. 3-10. For a given temperature rise at the insulated rear face, a value of the dimensionless temperature rise $(t - t_1)/(t_i - t_1)$ can be computed. A value of Θ can be obtained from Fig. 3-10 corresponding to an X/L value of 0.5 and the temperature rise. Then a conversion from Θ can be performed as follows:

$$\Theta \equiv \frac{a\theta}{\delta_1^2}$$

$$E \equiv \frac{q_o \theta}{\rho \delta_1}$$

thus

$$E = \frac{q_o \Theta \delta_1^2 / a}{\rho \delta_1} \quad (3-2)$$

This calculation was performed using representative values for the 20 and 60 Btu/ft²sec heat flux conditions, and the results are shown in Fig. 3-13. This value of E applies only for the case of the 2 in. thickness used in these experiments; the meaning of a higher value of E in one case over another is that the time required for a given rear-face temperature rise is proportionately greater. It may be noted that E could have been calculated by eliminating thickness rather than time between the defining equations for H and E , and for

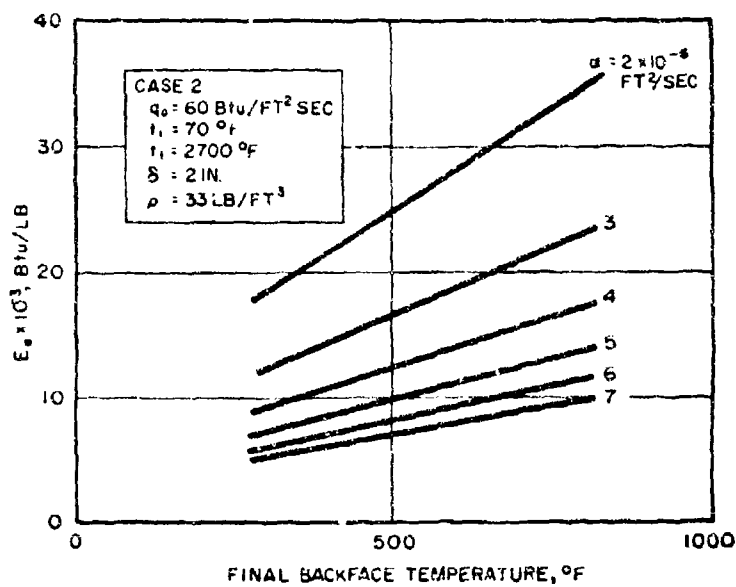
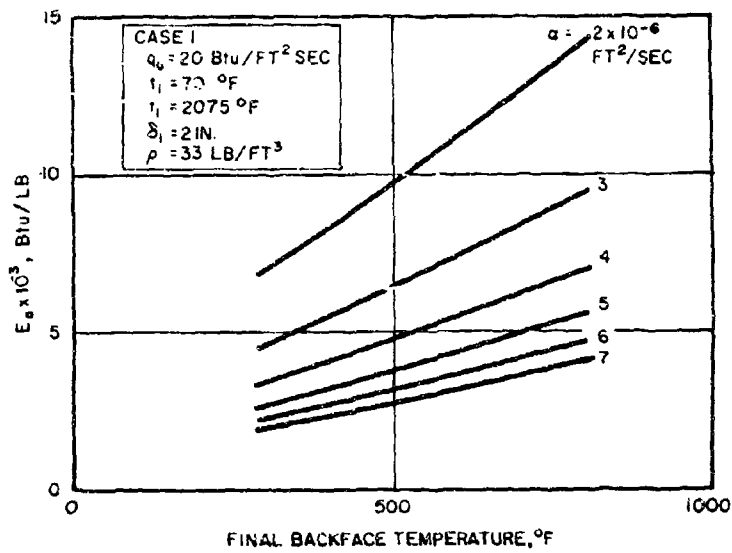


Figure 3-13. Theoretical Insulation Efficiency

that case a time-dependent E is obtained. The meaning of a higher value of E in this second, or time-dependent, case is that for a given exposure time less material (i.e., weight per unit surface area) is required to limit the rear-face temperature rise to the desired value. The constant thickness (and constant w/A since all materials had the same over-all density) value of E is preferred for the comparisons here because of the observed rise in apparent diffusivity during some of the tests and is discussed in more detail below.

The comparisons shown in Fig. 3-11 (to obtain an apparent diffusivity) and the efficiency results of Fig. 3-13 were used to determine an ablation efficiency E_a for the tests at 20 and 60 Btu/ft²sec heat flux. This efficiency is shown in Fig. 3-14 for each material calculated for diffusivities apparent at 300 and 600 sec to indicate any trend with time which might exist.¹ With few exceptions, the efficiency appears constant at the lower heat flux level. However, several materials exhibit decreases with time at the 60 Btu/ft²sec condition.

Figure 3-14 shows the analyzed insulation results of these tests in a practical form and merits some study. First, it is apparent that in general the efficiency E_c rises in almost direct proportion to the cold-wall heat flux. This is in agreement with recent studies of this class of ablators and results from the relative insensitivity of surface temperature to heat flux and the predominantly conductive character of the internal processes. Next, several materials exhibited considerable data scatter. It remains to be determined whether this scatter was caused by random differences in the raw material used or in spurious changes in the test condition. A notable result is that, referring to the effective diffusivity scale on the right in Fig. 3-14, most materials exhibited a diffusivity value about equal at both heat flux levels.

The fact that some materials showed a decrease in insulation efficiency with increasing time is probably significant. First, it must be ascertained

¹Recent additional tests have been performed which show results similar to these, except for an indication of somewhat better thermal performance of materials 5 and 8 at the lowest heat flux level.

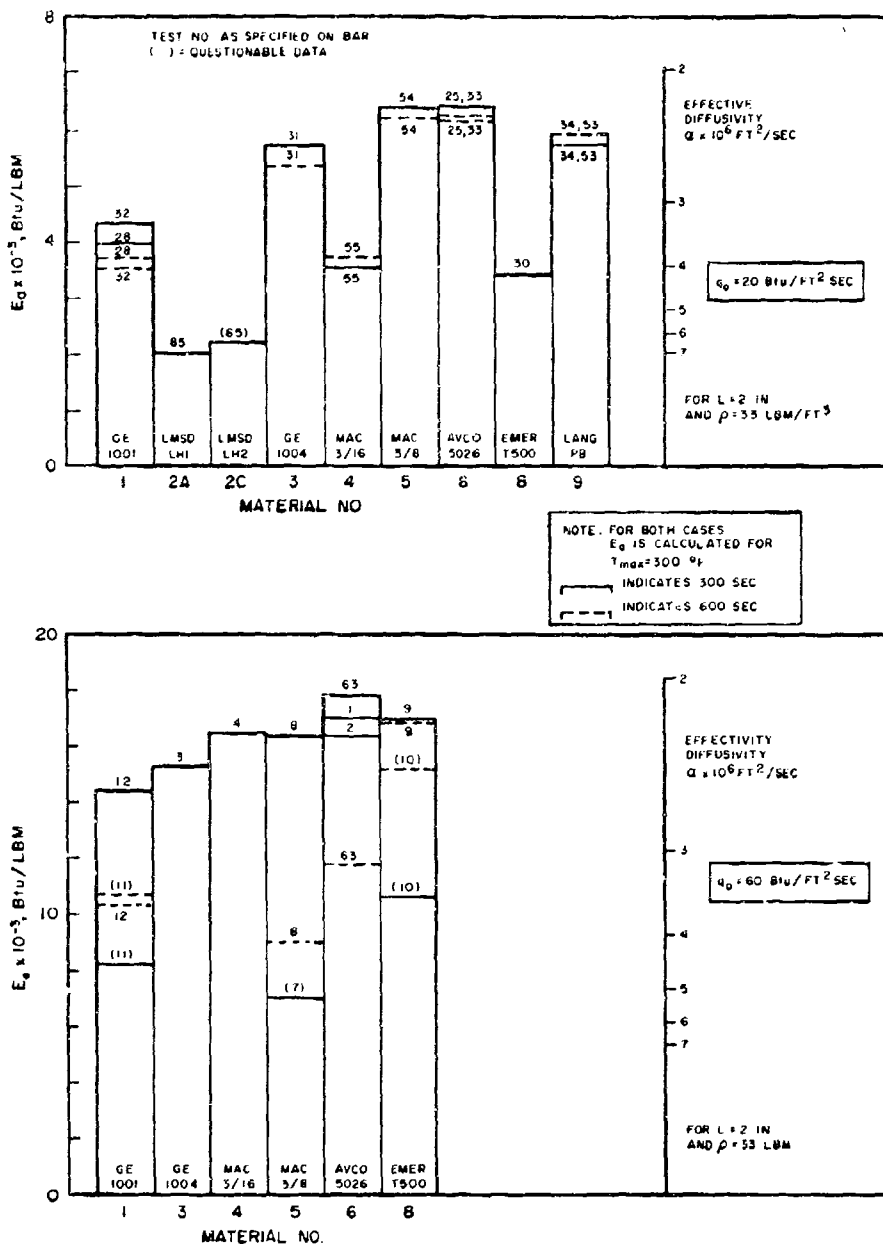


Fig. 3-14. Experimental Insulation Efficiency

whether this is a real characteristic which is not at least in part due to side-heating effects. Further tests, including measurements of specimen-periphery temperatures, are required to establish the influence of side heating. If it is found that the effect is not spurious, then it will be necessary to perform additional tests for longer heating durations and different specimen thicknesses than used in the present tests to establish the nature and magnitude of the change in apparent diffusivity for practical applications. If one refers to Table 3-1, it may be noted that at the end of 600 sec for the 60 Btu/ft²/sec heat flux case most materials had formed a char layer of appreciable thickness compared to the 1 in. depth of the internal thermocouple. This may account for the rise in apparent diffusivity noted in the tests, and may also suggest that had the tests been continued for longer durations even more significant changes in apparent diffusivity and efficiency would have resulted. For this reason, the present results should be viewed with some caution and emphasis should be placed on resolving these problems with additional tests and analysis. The efficiency calculation was made only for the 2 in. material thickness rather than extending the results to an arbitrary thickness, since the ratio of char thickness to total thickness could have a large influence on the proper value of apparent diffusivity to be applied.

The effect of (spurious) rear-face heating can be observed in Fig. 3-15, which compares the measured temperature rise at $q_0 = 20$ Btu/ft²/sec with theoretical values for the appropriate range of thermal diffusivity. Here the measurements correspond to diffusivities generally between 4 and 7×10^{-6} ft²/sec, whereas the previous discussion of measurements at the 1 in. depth has indicated diffusivities generally between 2 and 4×10^{-6} ft²/sec. This discrepancy is indicative of some spurious heating of the rear face even in the tests after 34, which included improved insulation of the specimen and holder periphery. However, the rear-face temperature rise was thus limited to a sufficiently low level to eliminate a corresponding error in the temperature at the mid-depth position.

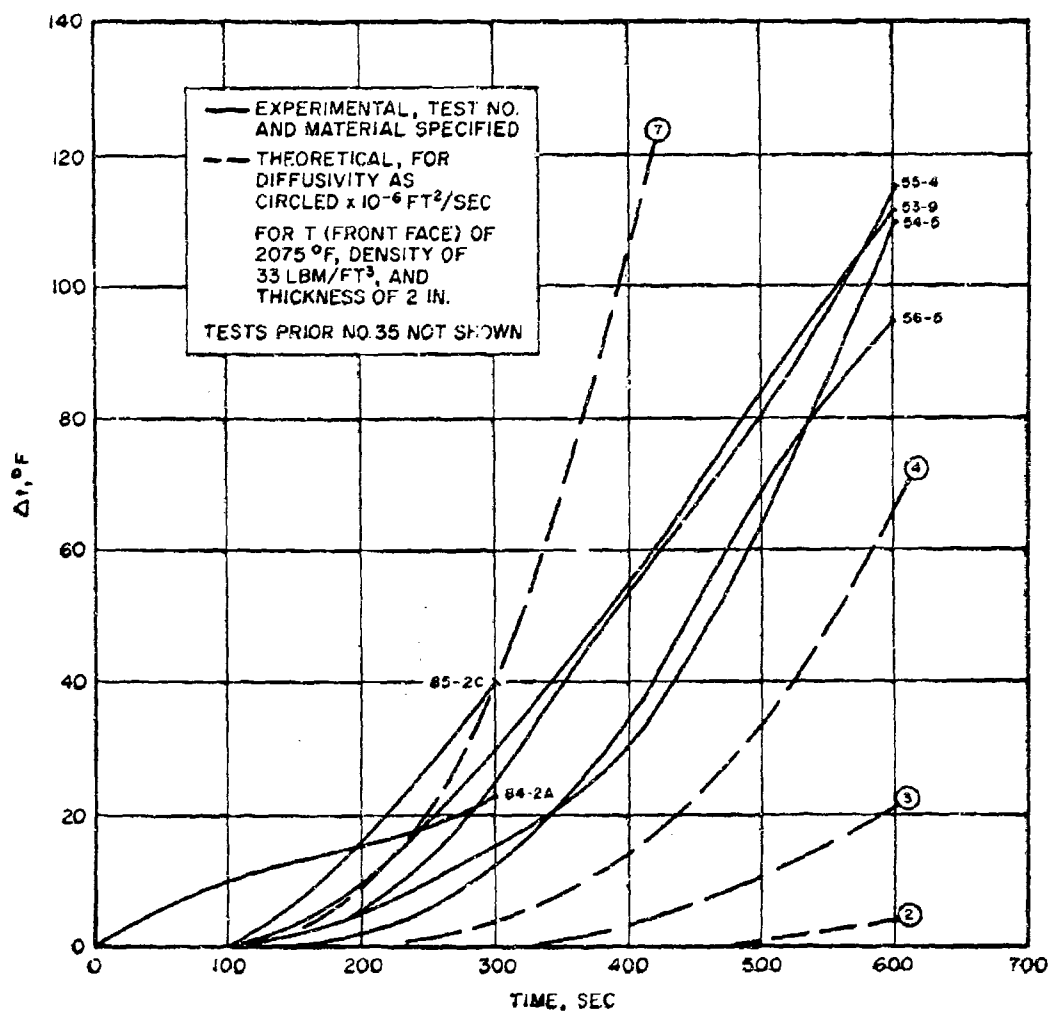


Fig. 3-15. Rear-Face Temperature Rise, $q_0 = 20 \text{ Btu/ft}^2\text{sec}$

VI. RECESSION ANALYSIS

At (cold wall) heat flux levels above $60 \text{ Btu/ft}^2\text{sec}$, all of the materials receded sufficiently to change the specimen thickness appreciably within the established test duration. No conduction analysis has been performed for these higher heat flux tests because of this complication of variable thickness and the lack of a convenient analytical solution for this condition. It is apparent that the insulation effectiveness for the receding case would be a decreasing function of time, however, based on the initial thickness.

This is primarily a comparative study of low density ablators; therefore it is of interest, even in the absence of a satisfactory correlation of recession performance, to compare the observed recession rates. The measured recession rates, shown in Fig. 3-1, are remarkably uniform for each of the three higher heat flux levels. The greatest variations from a mean recession rate are at the $90 \text{ Btu/ft}^2\text{sec}$ heat flux, where the data fall within a $\pm 40\%$ band. The data fall within a $\pm 32\%$ band at the 120 and 150 $\text{Btu/ft}^2\text{sec}$ heat flux levels.

A possibly significant exception to the uniformity of recession performance is that materials 6 and 8 showed measurable recession at the $60 \text{ Btu/ft}^2\text{sec}$ heat flux level where the other materials did not recede. This indicates a problem for further study; namely, the determination of the critical heat flux level at which each material begins to recede. A material with a critical heat flux of $80 \text{ Btu/ft}^2\text{sec}$ would be preferable to one of $40 \text{ Btu/ft}^2\text{sec}$, for example, if all other characteristics are equal.

An additional comparison of the measured surface-recession rates is shown in Fig. 3-16. Here the recession rate is normalized by the ratio of the calorimeter heat flux to the stagnation enthalpy (which is defined as $\rho_e u_e C_{H,O}$ in re-entry heat transfer calculations). This is done to identify the materials that act as charring and burning ablators. The charring ablator, at a sufficiently high surface temperature, will recede at a rate

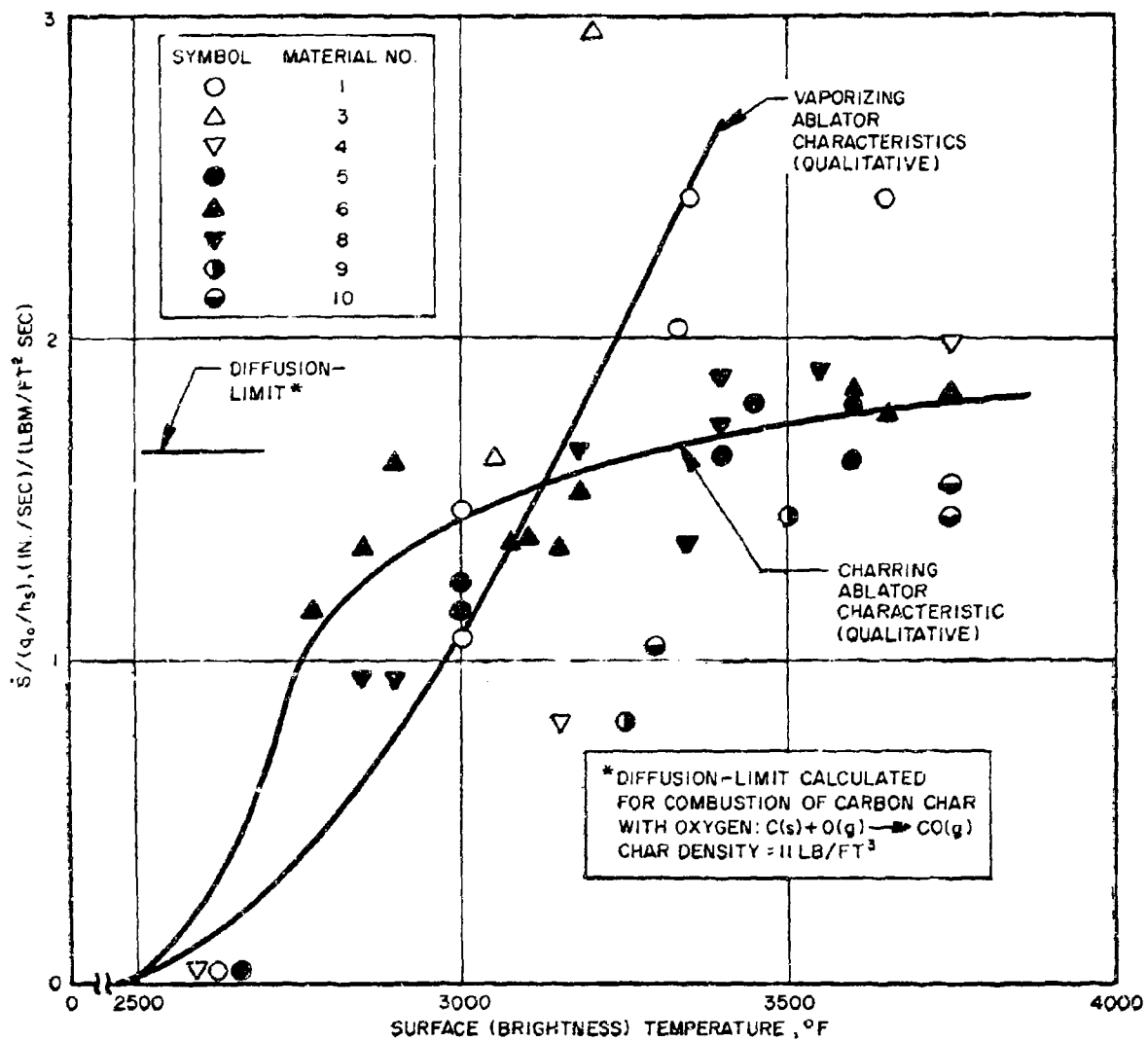


Fig. 3-16. Recession Characteristics

limited by the oxygen diffusion rate across the boundary layer (Ref. 3-3) given by the following relation:

$$\dot{s} = \left(\frac{K}{\rho_c} \right) C_{O_2, e} \rho_e u_e C_{H, O}$$

where

K = a coefficient which includes blowing effects

ρ_c = char density

$C_{O_2, e}$ = oxygen concentration in the freestream

$\rho_e u_e C_{H, O} = q/h$, heat transfer coefficient

At lower surface temperatures the surface combustion will be reduced from this diffusion-limited value, due to heterogeneous kinetic effects. A typical diffusion-limited value calculated for a char of 11 lb/ft³ is shown in Fig. 3-16 for comparison, based on the conditions of these tests. Several materials, 5, 6, and 8 in particular, exhibited recession rates which are asymptotic to the predicted diffusion-limited value. However, most of the materials showed no tendency to become diffusion-limited at high surface temperatures, and it is presumed that these materials recede through a vaporization process at the heated surface. Approximate characteristic curves for each class are also shown in Fig. 3-16.

VII. SHEAR TESTS

A single shear test was performed for nine of the materials using a 1 in. thick, 2 in. diam specimen inserted flush with one face of a 15 deg-half-angle wedge. The wedge was a water-cooled copper block with a leading edge of 1/8 in. radius. A transition ring of phenolic nylon was installed between the wedge and the specimen. This ring had a 3 in. o.d. and a 2 in. i.d. and was 1/2 in. thick; it was fitted flush with the wedge surface. One internal

thermocouple was installed at a depth of 1/2 in. in the specimen. A small calorimeter plug was installed flush with the specimen surface to monitor the surface heat flux.

Tests were performed at an estimated aerodynamic shear level of 2 lb/ft². The calorimeter plugs indicated a cold-wall heat flux of 30 Btu/ft²sec. A Reynolds' analogy calculation was made to deduce the actual aerodynamic shear level, 1 lb/ft².

Results are not shown for the shear tests because they are invalid. The phenolic nylon mounting ring, also exposed to heating and shear, became badly damaged early in each test. This mounting ring damage so roughened the surface contour as to cause separated flow and a shock wave just upstream of the specimen. The Reynolds' analogy calculation of shear was thus invalidated. It may be noted that the specimens showed negligible recession in the tests.

VIII. SUMMARY

Eighty-nine arc-tunnel tests have been performed in a survey of available low density materials for thermal protection of ablative lifting reentry vehicles.

Most of the tests were in the thermal series, in which flat-faced cylindrical specimens were tested for times up to 975 sec to determine recession rates and insulation qualities of the 10 materials. Front-surface brightness temperature was measured. Results have been summarized for recession, internal temperature (1 in. depth), and rear-face temperature responses. It was concluded that rear-face temperatures may not be meaningful for these tests, but that the internal temperatures shown are valid in most cases.

A small number of tests were performed to determine the sensitivity of these materials to aerodynamic shear, but that series was unsuccessful.

The materials tested were found to have internal temperature responses in the nonrecession regime similar to pure heat conductors with thermal diffusivities between 2 and 7×10^{-6} ft²/sec. The apparent diffusivity tended to increase with time, and the corresponding insulation efficiency decreased with time.

In the recession regime all materials (except 2A and 2C which became distorted and are excluded from discussion) showed comparable recession rates at a given heat flux within 40% of a mean value. Materials 6 and 8 began to recede appreciably at the 60 Btu/ft²sec heat flux, whereas the other materials showed no recession until the 90 Btu/ft²sec condition was imposed.

REFERENCES

- 3-1. "Materials Testing Program for Aerospace Corporation," under Contract AF 33(657)-8476, Dec. 21, 1964 through Jan. 11, 1965, Special Projects Group, Giannini Scientific Corp., Santa Ana, Calif. (January 1965).
- 3-2. P. J. Schneider, Conduction Heat Transfer. Addison-Wesley, Cambridge, Mass. (1955).
- 3-3. S. Lafazan and W. E. Welsh, Jr., "The Charring Ablator Concept; Application to Lifting Orbital and Superorbital Entry," Dynamics of Manned Lifting Planetary Entry, ed. Scala, Harrison, and Rogers, J. Wiley and Sons, Inc., New York (1963).
- 3-4. R. T. Swann, M. B. Dow, and S. S. Tompkins, "Analysis of the Effects of Environmental Conditions on the Performance of Charring Ablators," Proc. AIAA Entry Technology Conf. Oct. 12-14, 1964, pp 256-269.

PART 4. SUMMARY AND CONCLUSIONS

I. SUMMARY

Most ablative materials, e.g., phenolic nylon, phenolic graphite, phenolic carbon, and phenolic reffrasil, have been developed for high heating rates, high shears, and the short times characteristic of ballistic reentry and rocket nozzle environments. In these applications, surface recession rates in critical areas largely control backface temperature response. Thus, the high heating rate materials are relatively dense for minimum weight loss by shear, etc., and for minimum thermochemical surface recession. However, for the low heating rate, long time heat pulse experienced by ablating lifting bodies insulation properties dominate materials performance. Surface recession still is influential, but its significance is much less than for the higher heating rate environments. Therefore, new criteria are required for evaluating the performance and safety factors inherent in ablative lifting body thermal protection systems. In this new ablative application the primary materials properties which control backface temperatures and heat shield weights are the thermal conductivity and density.

In the present state of the art, the low density ablators that formulate at about 32 lb/ft³ appear to represent an empirical optimum based on configuration, fabrication, reentry environment, and system performance requirements. It is anticipated that as a result of continuing Air Force and NASA development programs, further materials improvements and more efficient utilization will occur through improved thermostructural design, development of refurbishment techniques, etc.

The application of low density refurbishable panels to lifting bodies in the high L to D class (supersonic $L/D > 3$) is possible through the integration of ablative and reradiative structures. Further improvements in recession and thermal performance will enhance the application of low density materials to all types of reentry vehicles. For example, the low density materials

could be used for the Gemini reentry environment with a 50-75 lb weight saving in the heat shield. Applications to low heat flux areas of ballistic systems also exist.

As shown by the data in Part 3, the materials tested have insulating characteristics comparable to idealized heat conductors with thermal diffusivities between 2 and 7×10^{-6} ft²/sec under test conditions producing no recession. Thus, there may be a significant difference in thermal performance of the low density materials; however, for application to a specific system it is necessary to include all of the aspects of environment, configuration, fabrication process, performance, and quality control before making a materials selection.

As deduced from the one-dimensional heat conduction analysis of the time-temperature response in Part 3, the apparent diffusivity had a tendency to rise during some tests. The char in some materials apparently have a higher conductivity due to a higher char density or to other effects, e.g., increased radiative heat transfer in the porous structure as the char layer thickens. The char density of the materials tested varied from 10-11 lb/ft³ at the char layer interface to 25-30 lb/ft³ at the hot face for materials with considerable hot-face pyrolytic deposition. These data are believed to be typical of the changes that occur in low density ablators with a high percentage of low density fillers.

The hot-face density increase is a characteristic of the silicone elastomeric materials and illustrates how pyrolytic deposition and sintering or shrinkage at the hot face can change the char thermal properties and material performance for a given environment. Since these changes are not understood the effects should be evaluated for complete materials optimization. Materials with finer pore size fillers, lower density, lower char density, and new types of fillers should be evaluated.

In order to understand the surface recession performance of the elastomeric materials as compared to charring ablators, the tests described in Parts 2 and 3 were supplemented by tests at high heat flux. These tests were run under conditions similar to those described in Parts 2 and 3 and will be

reported at a later date in conjunction with C-SiO₂ char chemistry studies. These data, summarized in Fig. 4-1, are shown in comparison with the data of Parts 2 and 3 which are represented as bars at the various heat fluxes. The high heat flux data reveal specific trends in the recession performance of the elastomeric materials as compared to charring ablators. The silicone materials do not recede until the heat flux exceeds about 90 Btu/ft²sec while the charring ablator materials show lower recessions above approximately 90-120 Btu/ft²sec as illustrated by the lower curve in Fig. 4-1.

The high heat flux data for the plasma tests shown in Fig. 4-1 show that silicone elastomers display characteristics of subliming or reaction rate controlled ablation above 90 Btu/ft²sec. Under the low pressures of these simulated environmental test conditions, silicone materials form a protective melt-layer below 60 Btu/ft²sec but not at the higher heat fluxes.

It is apparent that the charring ablator materials are more efficient for the high heat flux, short reentry times while the silicone elastomers are more efficient for the milder heat fluxes and longer reentry times. The data of Fig. 4-1 further suggest that it is possible, by judicious formulation, to obtain an optimum ratio of SiO₂-C in the char so that one might achieve low recession at low heat flux and charring recession rates at high heat flux.

Despite the high recession rates experienced by the silicone elastomers at the high heat flux it was concluded from these plasma tests that the silicone elastomer ablation materials are a good choice for present and future mission requirements for ablative lifting bodies. This conclusion is based on thermal performance, insulation efficiency, recession characteristics, cold soak properties, manufacturing simplicity, materials availability, reliability for the mission requirement, and process and quality control procedures.

For comparison, the calculated and measured oxygen diffusion limited recession rates for a charring ablator (material 6 char density, 11 lb/ft³) are indicated in Fig. 4-1. The recession rate for the elastomeric materials exceeds the maximum rate for surface combustion-controlled recession. These data indicate a need for further understanding of the kinetics of char and ablation chemistry to establish the temperature and oxygen pressure

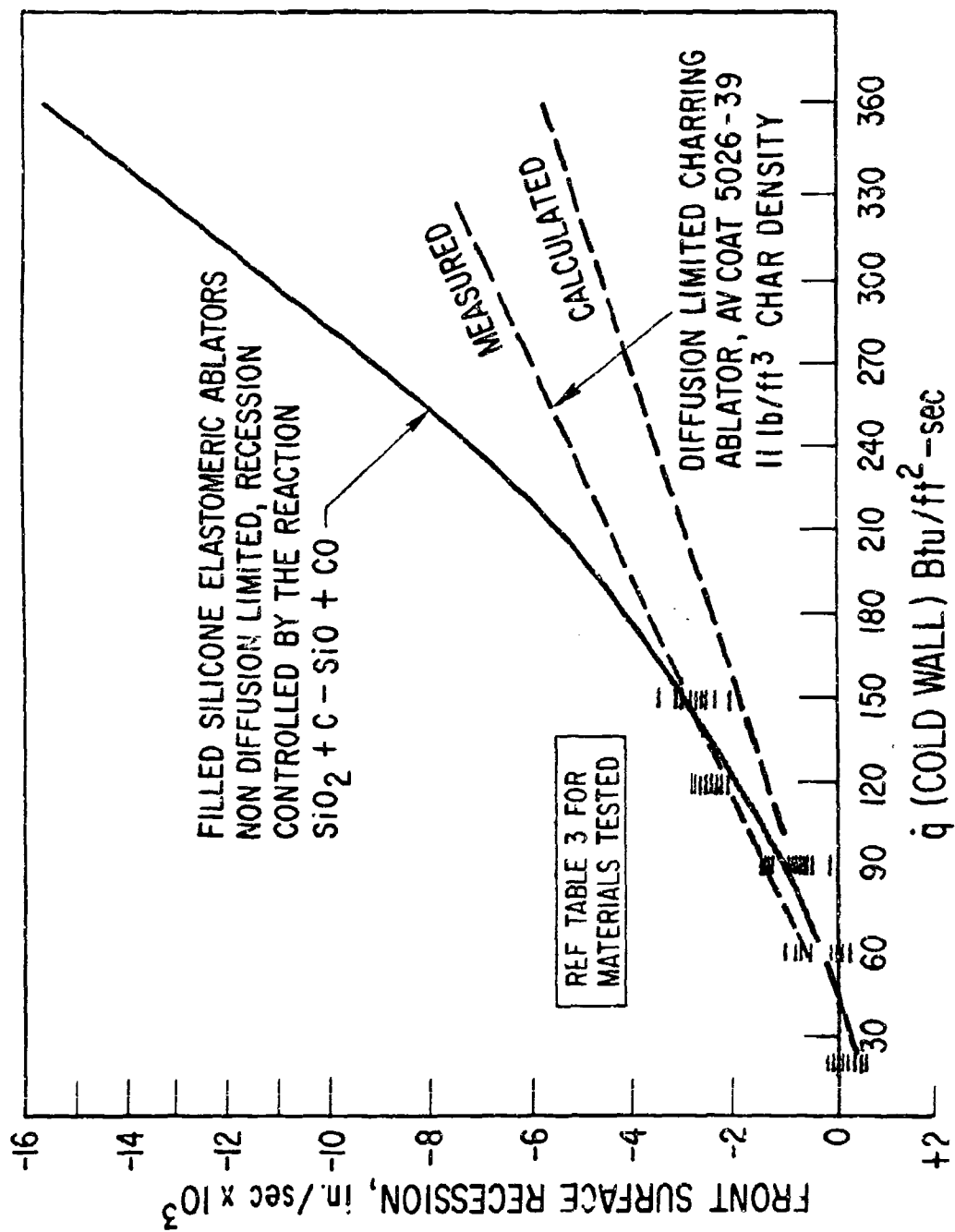


Fig. 4-1. Recession Characteristics of Low Density Ablators (32 lb/ft³)

dependence of recession rate for silicone elastomers. Such studies are in progress in this Laboratory, and the preliminary data and conclusions are reported below.

Mass-loss studies carried out at a pressure of 0.033 atm and at varying oxygen partial pressures over a temperature range from 1300 to 1550°C have shown (Table 4-1) that a 1% oxygen partial is required to suppress the ablation process which is assumed to take place by reaction (2) below.

An apparent activation energy of 113 kcal/mole was obtained for this reaction from the rates of CO formation (Table 4-2). The rate of this reaction becomes appreciable, and the formation of SiO is indicated as evidenced by the destruction of platinum furnace parts due to the reaction between platinum and gaseous silicon monoxide to form platinum silicides. These studies will be completed and reported at a later date.

Although it has not been possible to develop specific rate constants for use in charring ablator computer programs, it is possible to state that there are principally two reactions that occur:



In general, reaction (1) occurs at temperatures below about 1350 to 1400°C, whereas reaction (2) predominates at higher temperatures and at low oxygen pressures. Studies are in progress to identify the reaction products and to determine the effect of oxygen pressure and C-SiO₂ ratio on recession rate.

The formulation of most silicone elastomeric materials is such that after charring at temperatures to 1000°C the char is composed predominately of SiO₂ and C, which do not react further at an appreciable rate until a temperature of 1400°C is reached at low oxygen pressures. Chars prepared in the laboratory by heating in argon at 600°C and then heating at low oxygen pressure at temperatures above 1500°C (2732°F) sublime and leave less than 3% residue based on the original virgin weight, as shown in Table 4-2.

Table 4-1. Mass-Loss Data on Charred Silicone Elastomer at 0.033 atm

Partial Pressure of O ₂ , mm Hg	% Weight Loss			
	1300°C	1400°C	1500°C	1550°C
0	30	>85	>95	>95
0.125	31	37	42	60
0.25	32	33	34	34
0.50	33	33	--	--
1.25	33	33	33	--
2.5	32	33	33	--
5.0	33	33	34	--

Note: Material was charred at 600°C to give a mixture of SiO₂ and C.

Table 4-2. Rate Data on Charred Silicone Elastomer at 0.033 atm

T, °K	1/T × 10 ⁴ , °K ⁻¹	Rate × 10 ⁵ , gm CO sec ⁻¹
1646	6.075	0.507
1674	5.974	0.868
1685	5.935	1.197
1703	5.872	1.85
1712	5.846	1.95
1733	5.770	2.93
1781	5.620	9.0
1781	5.620	7.0
1823	5.485	10.0

Note: Material was charred at 600°C to give a char containing amorphous C and SiO₂.

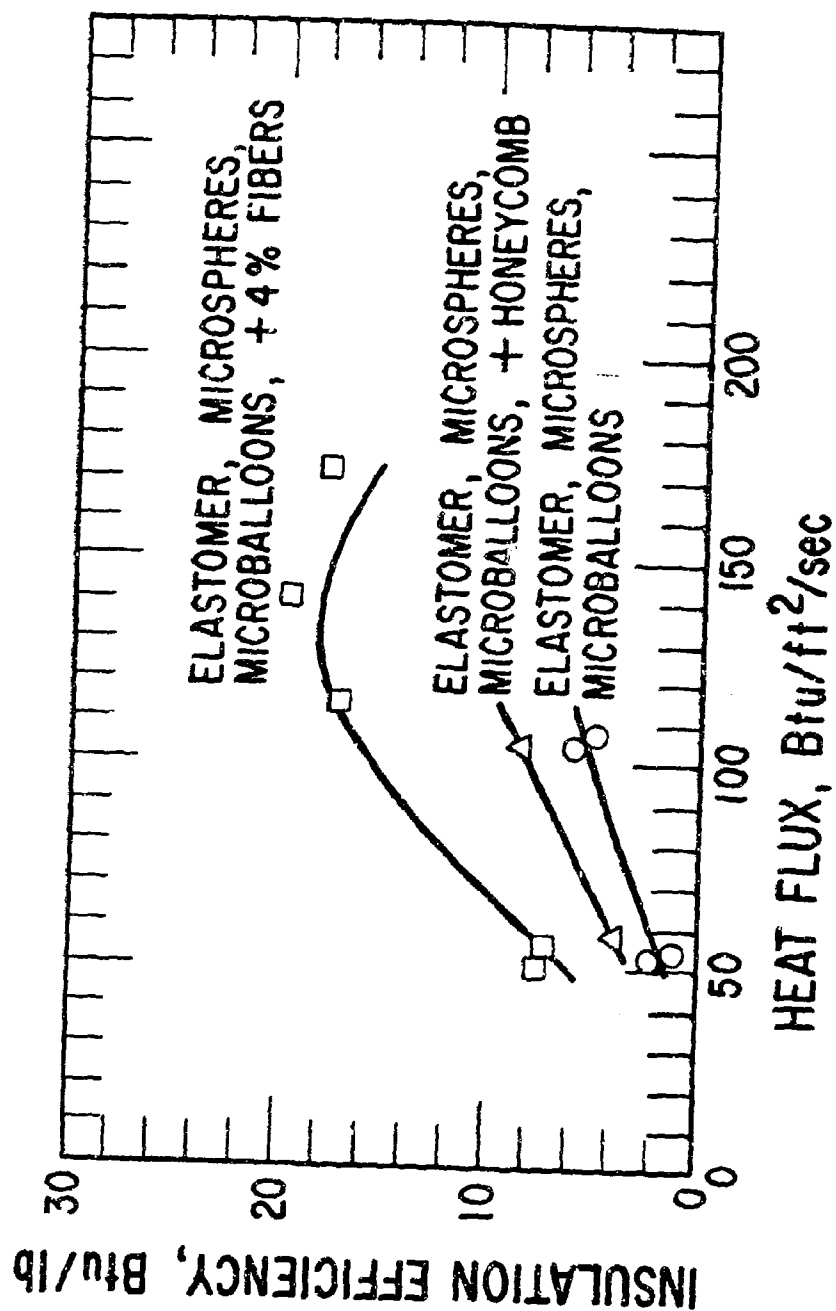


Fig. 4-2. Insulation Efficiency of NASA/Langley Purple Blend with Fiber Addition
(from R. Clark, Environmental Parameter Effects on
Performance of Low Density Silicone-Resin and
Phenolic-Nylon Ablation Materials,
NASA TN-D-2543, January 1965)

The thermochemical behavior of the silicone chars in the plasma tests reported in Part 3 and in the laboratory data presented in Table 4-2 is consistent with the thermodynamic data for reaction (2) reported by Schick (Ref. 4-1) and Edwards and Brewer (Ref. 4-2) and the kinetic data reported by Rosensweig and Beecher (Ref. 4-3) and Blumenthal, Santy, and Burns (Ref. 4-4).

The pronounced increase in insulation efficiency resulting from the addition of fibers to elastomeric ablators as reported by Clark (Ref. 4-5) and shown in Fig. 4-2 was not reflected in any of these materials which were formulated at 32 lb/ft^3 . Possibly the failure to observe this effect was due to the effect of oxygen pressure on reactions (1) and (2), to an overriding effect of density on ablation performance, or to differences in test conditions. In contrast to the 32 lb/ft^3 for the silicone materials tested in our program, the data reported by Clark (Ref. 4-5) were determined for materials having a nominal density of approximately 45 lb/ft^3 and formulated with quite different percentages of fillers. Also, the tests described in this report were carried out in a low pressure ($< 0.1 \text{ atm}$), supersonic plasma as compared with the 1-2 atm subsonic plasma used by Clark.

Equilibrium data (Ref. 4-1) for reaction (2) indicate that the dissociation pressure of SiO and CO exceeds the plasma test pressures as reported in Part 3 at temperatures above about 1400°C (radiation equilibrium heat flux $39 \text{ Btu/ft}^2\text{sec}$) at pressures below 0.1 atm . As noted earlier, the elastomeric materials showed a significant recession at low pressures only at heat fluxes greater than $60 \text{ Btu/ft}^2\text{sec}$ corresponding to 1600°C radiation equilibrium temperature. Similarly, under Clark's (Ref. 4-5) test conditions (assumed 1 atm) the equilibrium CO dissociation pressure would exceed the test pressure at approximately 1600°C which is 300°C lower than the calculated radiation equilibrium temperature, 1900°C , corresponding to the 100-125 $\text{Btu/ft}^2\text{sec}$ heat flux (Fig. 4-2) above which Clark reported an increasing recession rate. Thus, it would appear that reaction rates and mass transport cause the observed elastomeric char thermochemical behavior to lag equilibrium prediction by $200\text{-}300^\circ\text{C}$. Additional analysis is needed to clarify the

interpretation of data; however, it appears that thermochemical effects are significant and may be dominant in the optimal performance demonstrated by the data in Fig. 4-2.

Although it is not possible to define precisely the effect of aerodynamic shear on the integrity and performance of low density materials at this time, data from other sources indicate that the effect of shear is negligible for the expected flight environment. Further quantitative tests will be conducted in the future.

II. CONCLUSIONS AND RECOMMENDATIONS

The materials tested in this report indicate that there are several commercially available materials that can meet the thermal performance requirements for ablative lifting bodies, e.g., M-2, HL-10, and SV-5.

The data presented in Table 4-2 in which silicone elastomeric chars were heated over a range of temperatures and oxygen pressures demonstrate that the recession performance of this class of materials depends primarily on temperature and oxygen pressure and also on density and C-SiO₂ ratio.

Silicone elastomers as a materials class for ablative lifting bodies are convenient to process and have superior recession performance for mission requirements not exceeding 90-120 Btu/ft²sec. Charring ablators, for example, Avco 5026-39, show diffusion limited recession rates which are lower than the silicone elastomers for heat fluxes above the 90-120 Btu/ft²-sec range for typical lifting body environments.

The supplementary data shown in Fig. 4-1 and Table 4-1 suggest that a low density silicone elastomer ablator with a high carbon content char might have a better recession and thermal performance over a wider heat flux range as compared to the elastomeric materials evaluated in this program.

Continued systems-oriented studies are required to develop the optimum combination of design, fabrication, and ablation materials use for minimum weight and for refurbishable lifting bodies.

The recession and thermal performance of low density ablators suggests that these materials in combination with reradiative panels and high density ablators have potential application for high L to D vehicle leading edges and other areas with heat fluxes above the 40 Btu/ft²sec operating limit for coated refractory metals.

Thermostructural studies are required to determine optimum methods for combining refractory metal re-radiative and ablative systems for lifting reentry for both high and low L to D lifting bodies.

Low density ablation materials have potential systems applications for thermal insulation in other aerospace systems.

REFERENCES

- 4-1. H. L. Schick, "A Thermodynamic Analysis of the High-Temperature Vaporization Properties of Silica," Chem Rev. (Aug 1960).
- 4-2. L. Brewer and R. K. Edwards, "The Stability of SiO Solid and Gas," J. Am. Chem. Soc. 58, 351 (1954).
- 4-3. R. E. Rosensweig and N. Beecher, "Theory For The Ablation of Fiber-glas-Reinforced Phenolic Resin," AIAA J. 1, 1802 (1963).
- 4-4. J. L. Blumenthal, M. J. Santy, and E. A. Burns, "Kinetic Studies of High Temperature Carbon-Silica Reactions in Charred Silica-Reinforced Phenolic Resins," Paper presented at Western States Section, The Combustion Institute Fall Meeting, Oct. 1965 (Paper No. WSCI 65-25).
- 4-5. R. Clark, Environmental Parameter Effects on Performance of Low Density Silicone-Resin and Phenolic-Nylon Ablation Materials, NASA TN-D-2543 (Jan. 1965).